IDEA League

Master of Science in Applied Geophysics

Research Thesis

Detection of cavities in levees caused by the muskrat and other mammals by use of geophysical methods

Marijn Benthem

August 7, 2015

TU Delft
Delft University of Technology

Deltares
Enabling Delta Life

Detection of cavities in levees caused by the muskrat and other mammals by use of geophysical methods

Master of Science Thesis

for the degree of Master of Science in Applied Geophysics at
Delft University of Technology
ETH Zürich
RWTH Aachen University
by

Marijn Benthem

August 7, 2015

Department of Geoscience & Engineering · Delft University of Technology
Department of Earth Sciences · ETH Zürich
Faculty of Georesources and Material Engineering · RWTH Aachen University

Delft University of Technology

Printed in The Netherlands, Switzerland, Germany

IDEA LEAGUE
JOINT MASTER'S IN APPLIED GEOPHYSICS

Delft University of Technology, The Netherlands
ETH Zürich, Switzerland
RWTH Aachen, Germany

Dated: *August 7, 2015*

Supervisor(s):

Victor Hopman

Prof. Evert Slob

Committee Members:

Victor Hopman

Dominique Ngan-Tillard

Prof. Jan van der Kruk

Contents

Samenvatting III

Abstract IV

Acknowledgements V

List of figures VI

List of tables X

1. Introduction 1

2. The muskrat problem 3

2.1 Damage caused by the muskrat 3

2.2 Muskrat management 3

2.3 The problem worldwide 5

3. A geophysical approach 6

3.1 Ground penetrating radar 6

3.2 Geo-electric methods 6

3.3 Electromagnetic method 7

3.4 Seismic tomography 7

3.5 Infrared thermography 8

3.6 Remote sensing 8

3.7 Carbon dioxide emission 8

3.8 Overview of methods 9

4. Ground penetrating radar 10

4.1 Background theory 10

4.2 PulseEKKO PRO 11

5. Electrical resistivity tomography 13

5.1 Background theory 13

5.2 SuperSting R8 14

6. Sites of investigation 16

6.1 Oostvaardersdijk, Flevoland 16

6.2 Alblasserwaard, South Holland 17

6.3 Wapenveld, Gelderland 18

6.4 Remarks on sites of investigation 19

7. Data processing 20
7.1 Processing the GPR signal 20
7.1.1 Basic handling in EKKO_Project 20
7.1.2 3D imaging in Voxler 23
7.2 ERT processing 24
7.2.1 Inverse modelling 24
7.2.2 Forward modelling 25
7.2.3 Data misfit analysis 26

8. Results and interpretations 27
8.1 Artificial tunnel at Wapenveld 27
8.1.1 250 MHz antenna 27
8.1.2 500 MHz antenna 28
8.1.3 1000 MHz antenna 28
8.1.4 Provisional conclusion 29
8.2 GPR and ERT in sand at the Oostvaardersdijk 29
8.2.1 Focus on entrance at waterside 29
8.2.2 The flat part of the bank 31
8.2.3 Detection when surveying large area 33
8.2.4 Interpreting ERT sections 34
8.3 Peat and clay at the Alblasserwaard 36
8.3.1 Location 1 36
8.3.2 Location 2 37
8.3.3 Location 3 39
8.4 Discussion 39

9. Conclusions 42

References 43

Appendix 46
Appendix A Cross-section Oostvaardersdijk 46
Appendix B Influence of SEG2-gain parameters 47
Appendix C Apparent resistivity section of the Wenner survey 48
Appendix D Alblasserwaard Location 1 raw data 48

Samenvatting

Een groot scala van wilde dieren leeft in en rondom dijken en oevers, waar ze door hun gebruik zodanige slijtage en schade aan kunnen richten dat de stabiliteit van de dijk in gevaar wordt gebracht. De muskusrat is in Nederland wijdverspreid en wordt al decennia intensief bestreden vanwege zijn grootschalige graverij. De methode van bestrijding is de laatste jaren steeds efficiënter geworden en de schade beter geregistreerd, waardoor de populatie sinds 2004 sterk gedaald is en ondertussen stabiel. Desondanks komt er vanuit de media en de samenleving steeds meer weerstand tegen het doden van de dieren en is er vraag naar een nieuwe vorm van beheer.

Dit onderzoek bekijkt vanuit verschillende geofysische invalshoeken naar de mogelijkheid om de holen, ook wel bouwen genoemd, op te sporen en in kaart te brengen. Diverse methoden zijn geëvalueerd op het detecteren van kleine holtes in de ondiepe ondergrond, waarbij de voor- en nadelen voor toepassing in het field zijn afgewogen. Metingen zijn uitgevoerd op diverse locaties in het land, geselecteerd op de omvang van de schade, type dijk en oever, en de ondergrond. Met de grondradar is met meerdere frequenties gemeten (250, 500, en 1000 MHz) en de weerstandmethode is uitgevoerd met verschillende rangschikkingen van de elektroden (Dipole-Dipople en Wenner). Er is getracht de resultaten door middel van een handboring naar waarheid te toetsen. Verschillende tunnels, stenen, en bouwafval zijn hierdoor geïdentificeerd. Veel boringen leverde niet het gewenste resultaat op, anders dan de ondergrond werden er geen oorzaken gevonden voor de afwijkende signalen. Ook zijn er ingangen, door de bestrijders aangegeven aan de waterkant, niet weergegeven door de methoden. De beste resolutie gaf de grondradar met de 500 MHz antenne, waarmee de bouwen het duidelijkst onderscheidbaar waren van de omringende grond. Met de weerstandmeting lukte het niet om duidelijk een holte te identificeren noch om de omvang vast te stellen.

Wereldwijd veroorzaakt de graverij van diverse dieren ook veel schade en dat wordt in steeds meer landen als een probleem erkend. Een efficiënte methode om de tunnels en bouwen op te sporen waarmee de werklast van de bestrijders wordt verminderd is zeer gewenst. Het is een streven voor de toekomst om de huidige geofysische methodes te optimaliseren in het detecteren en het in kaart brengen van de ondergrondse gangenstelsels van dieren.

Abstract

A wide range of wildlife has their habitat around and within levees or other types of embankment structures. In the Netherlands the burrowing of the muskrat causes internal and external erosion, altering the geometry of the earthen structure. As often century-old embankments protect the densely populated land against the water, the burrowing can form a severe thread to the public safety. At present, the problem is managed by placing lethal and non-lethal capturing techniques in and around burrow founds by visual inspection. Although the population of the muskrat has been under control since 2004, a growing opposition of the media and public to the current control policy gives potential to a different way of monitoring embankments for animal cavities.

This research focuses on a geophysical approach to detect muskrat burrows and to visualize the spatial extent of the tunnel network. Various methods have been judged on their potential to image the shallow cavities and evaluated on their advantages and disadvantages for field application. As outcome, fieldwork has been conducted with ground penetrating radar using multiple frequencies (250, 500, and 1000 MHz) and electrical resistivity tomography using different array setups (Dipole-Dipole and Wenner). Sites of investigation have been chosen throughout the Netherlands with different sized and shaped embankments and soil constituents. To ground truth the observations, holes have been drilled by hand to confirm several anomalies. This resulted in identification of various animal tunnels, rocks and plastic debris. However many drilled holes did not yield the desired outcome and many anomalous reflections remained unidentified. Moreover some entrances indicated by the muskrat controllers have not been detected by the methods. The 500 MHz antenna showed the highest resolution in the shallow subsurface and has been the best in detecting and mapping the muskrat burrows. The resistivity arrays failed to clearly distinguish any cavity from the surrounding soil.

Organizations worldwide have reported similar nuisance activities of wildlife in dams and levee systems. An efficient instrument that reduces the labour-intensive management is highly desired. Optimizing geophysical methods, in particular the ground penetrating radar, for shallow small-sized cavity detection is a future interest.

Acknowledgements

This report is the outcome of the thesis of the IDEA League master program Applied Geophysics in collaboration between Deltares and the Technical University Delft, conducted from March till August 2015.

The main component of my research has been the field work, which included inquiring the scope of the muskrat problem and the acquisition of the geophysical data. Consequently, I had the pleasure to meet various different people and travel to many places in the Netherlands I had not been before. For this opportunity I would like to thanks those that have contributed to my research both directly and indirectly.

First of all I would like to thank the department Subsurface and Groundwater Systems at Deltares in Utrecht for giving me the opportunity to investigate the topic and providing me with all the material needed for my research. In particular I would like to thank my supervisor Victor Hopman for his constructive motivational guidance and Mike van der Werf for helping me with the equipment and software.

From the TU Delft I would like to thank Alber Hemstede for helping me with all my questions and instructions on the TU Delft material, Laura Konstantaki for her enthusiastic interest in my topic and assisting me with the ground radar processing software. Additional thanks go to Dominique Ngan-Tillard for guidance with the ground radar instruments and Evert Slob for being my principle supervisor.

Various muskrat management organisation have been very helpful with providing me information, showing me their way of working and taking me along into the field. Thanks go out to Zuiderzeeland and Michael Baars as they have been the first to respond and give me my first field impression. From muskrat management Rieverenland I would like to thank Anton Deelen and from Valei & Veluwe Lambertus van Diermen for showing me around in new locations and providing me with additional information.

Special thanks go out to Mike Lahaye, my fellow intern that accompanied me to nearly all my days in the field. I would not know how it otherwise would have taken shape as your enthusiastic interest in my topic and help encourage me with my struggles in the field. Thank you for your driving skills with both the car and the smartcart and your commitment to mow the high vegetation encountered.

Last but not least, I would like to thank my family for always being very supportive and motivating me for my first ever car drive alone. Finally I would like to thank my boyfriend Ingmar Barendregt for all the moral support and even accompanying me to the field for two days.

Marijn Benthem

August 2015, Utrecht

List of figures

Figure 1: Mounted beaver (left), muskrat (middle) and coypu (right). Their size in comparison to the muskrat indicates their significant larger burrowing 1

Figure 2: Map with the 8 Muskrat management organizations that operate in the Netherlands. The 3 areas at which the measurements of this research have been performed are indicated by stars. 2

Figure 3: Excavating PUR foam filled muskrat burrow with significant size reaching the crest of the embankment (Akkermans 2014) 3

Figure 4: National development of the number of muskrats caught per year. A sharp decrease after 2004 down to 100 000 appears to be stable (Union of Water Authorities 2015) 4

Figure 5: Muskrat controller inspects the waterside and places clamps indicated by an orange flag (Union of Water Authorities 2014) 4

Figure 6: Schematic depiction of hyperbolic response for a small point target, like a tunnel. 11

Figure 7: PulseEKKO Pro 250 MHZ antenna smartcart with GPS system later proved to be inaccurate 12

Figure 8: Schematic electrode setup of a Dipole-Dipole and Wenner array 14

Figure 9: SuperSting setup, with on the left the yellow cables connecting the electrodes with the swift box (middle below) and the SuperSting in the black open box. In the right lower corner the closed black box is the battery 14

Figure 10: Schematic depiction of measurement points using Dipole-Dipole array with $na = 6$ and $a = 8$, showing many points measured till depth of 2 electrode spacing's (dark blue and red). 15

Figure 11: Schematic depiction of measurements points using Wenner array with $a = 9$, showing less measurements points compared to Figure 10. In the field Wenner array was measured with $a = 6$, given a similar section but without the lowest four point line (green, yellow, red and light blue). 15

Figure 12: The Oostvaardersdijk with from left to right: water ditch, steep bank, flat bank and steep inside levee slope. In blue the outline of Grid 3 and the red arrow indicates the location the tunnel entrance found by the muskrat controller. 16

Figure 13: Overview of surveys measured at the Oostvaardersdijk 17

Figure 14: The narrow first location at Alblasserwaard with entrances at the waterside indicated by the orange flags. The white line denotes the 14 m surveyed line ending at the GPS. 18

Figure 15: Location 2 on a mound with entrances found around the tree. Flags are displaying the corner point of the 1.25 by 4 m grid measured with the 500 and 1000 MHz antenna. The high grass had to be mowed first to make it accessible for the GPR equipment. 18

Figure 16: Low vegetation at Location 3. The outer flags in the water are preventive clamps; the 3 middle flags (positioned in the grass) indicate the actual entrances 18

Figure 17: The grass field of Location 4 at Wapenveld with a muskrat entrance highlighted in red. The subsurface contained a too thick layer of clay 18

Figure 18: Steep embankment at Location 5 where a test hole (position denoted with a red circle) has been created to investigated response of the GPR 19

Figure 19: Line 7, trace 80 of Grid 3 measured with the 250 MHz antenna displaying various processing steps applied, black line indicates raw data; red line processed data; blue line indicates applied gain. Below processing steps are denoted with att=attenuation, start=start gain, max=maximum gain, window=window width: A)SEG2 (automatic parameters: att=11.35, start=4.49, max=477) (see Figure 20) B) SEG2 (att=11.35, start=4.49, max=477) + dewow (see Figure 21) C) SEG2 (att=11.35, start=4.49, max=477) + dewow + background removal (see Figure 22) D) SEG2 (att=11.35, start=1, max=477) + dewow + background removal (see Appendix B) E) SEG2 (att=11.35, start=15, max=477) + dewow + background removal (see Appendix B) F) SEG2 (att=20, start=4.49, max=477) + dewow + background removal (see Appendix B) G) SEG2 (att=11.35, start=4.49, max=1500) + dewow + background removal (see Appendix B) H) SEG2 (att=13, start=4, max=1500) + dewow + background removal (see Figure 23) I) AGC (window=1.5, max=500) + dewow + background removal (see Figure 24) 21

Figure 20: Radargram corresponding to Figure 19A with SEG2 gain applied, automatic parameters recommended by EKKO_Project. Wow dominates in deeper part. 22

Figure 21: Radargram corresponding to Figure 19B with SEG2 and dewow applied. Horizontal noise band is still present at around 30 ns, indicating a phantom reflection. 22

Figure 22: Radargram corresponding to Figure 19C with SEG2, dewow and background removal applied. Image contains less noise, the horizontal layer at 10 ns and the hyperbolic reflections (highlighted in orange) are more distinct. 22

Figure 23: Radargram corresponding to Figure 19H with SEG2 gain applied, parameters are chosen by the user to increase strength from signals at depth greater than 30 ns (highlighted in orange). 22

Figure 24: Radargram corresponding to Figure 19I with AGC, dewow and background removal applied. Relative signal amplitude is lost, especially in the upper 20 ns. The reflections are less distinct with AGC than with SEG2 applied. 22

Figure 25: Colour bars user for radargrams (bone) and slices (jet) 23

Figure 26: Scatter plot of GPR data made by Voxler of Grid 4 on the steep bank of the Oostvaardersdijk......... 23

Figure 27: Resistivity sections of Dipole-Dipole survey processed with EarthImager 2D. Top section depicts the measured apparent resistivity, middle section the calculated apparent resistivity from the bottom section. Parameters for inversion were a maximum RMS of 3% and a smoothing and damping factor of 10. Forward modelling was performed with the finite element method, using a Cholesky Decomposition forward solver equation and a mixed boundary condition. The upper two sections form a near exact resemblance and as such these parameters were chosen to fit best. 24

Figure 28: Convergence curve of resistivity inversion similar to Figure 27 but with no maximum value for the RMS error assigned. The graph shows that an acceptable RMS error is achieved after 5 iterations. 25

Figure 29: Data misfit scatter plot, showing high deviations mostly at data points on the right of the section.. 26

Figure 30: Data misfit histogram for removal of poorly-fit data. However in this case no points have been removed as the misfit values are acceptable. 26

Figure 31: Artificial tunnel in sandy soil at 20 cm depth. 27

Figure 32: Test line measured with the 250 MHz antenna shows no clear reflection within the orange highlighted area. The red box denotes survey line of Figure 33 and Figure 34 27

Figure 33: Survey line with artificial tunnel at 20 cm depth positioned at 2.7 m along the line. The orange circle indicates a weak hyperbolic reflection. 27

Figure 34: Metallic hand drill in the tunnel gives a strong distinct hyperbolic reflection with a left leg 27

Figure 35: Amplitude of signal at tunnel, positive peak when air-filled (left), negative peak when containing metal (right) 28

Figure 36: 500 MHz radargram showing weak reflection around 10 ns depth of tunnel without metal pole. 28

Figure 37: Two metal poles placed in the tunnel gives a strong hyperbolic reflection. Left axis with known depth of the tunnel estimate a 0.075 m/ns velocity ... 28

Figure 38: 1000 MHz survey line of the air-filled tunnel, no clear hyperbolic reflection. Highlighted in blue a vertical band of noise as result of poor ground contact. ... 29

Figure 39: Almost identical to Figure 38 despite a metal pipe placed in the tunnel ... 29

Figure 40: Soil sample drilled on the bank showing difference in the upper and lower sand. ... 29

Figure 41: Survey at 0.0m of grid, red lines indicated depth slice at 0.5-0.55m. Positive peaked hyperbolic reflections visible also at 2.5 m position. ... 30

Figure 42: Grid 4 at Oostvaardersdijk with an entrance (red) at waterside halfway the grid. ... 30

Figure 43: Line at 0.25m, hyperbolic reflections at similar positions as in Figure 44, they appear to continue .. 30

Figure 44: Horizontal slice at 0.5-0.55m depth, showing high amplitudes at position of a known entrance. 30

Figure 45: Line at 1.75m containing more reflections of which horizontal horizons and hyperbolic ones are less distinct. ... 30

Figure 46: Slice at 0.4-0.45m depth, strong amplitudes are more scattered and less continues. ... 30

Figure 47: 3D visualization of Grid 4 in Voxler with top view (upper image) and two side views (bottom images) showing a tunnel shaped structure starting at the half way the grid at the water side continuing upward the steep bank. ... 31

Figure 48: 3D visualization with left a lower isovalue showing more objects that cannot be related to a tunnel and right a higher isovalue gives a small volume. ... 31

Figure 49: 500 MHz radargram of line at 3.75 m position on vertical axis of Figure 50. For depth estimation a velocity of 0.06 m/ns was used as sand was found to be saturated. ... 32

Figure 50: Horizontal slice at depth 0.30-0.35 m showing a more continuous reflection. The steep part of the bank begins at 3.0m on the vertical axis of this grid and ... 32

Figure 51: Slice focused on hyperbole legs at depth 0.48-0.52 m (red lines Figure 49) with normal gain (upper) and extreme gain (lower) applied ... 32

Figure 52: Horizon is 3D visualized, it is impossible to identify hyperbolic reflections ... 32

Figure 53: 500 MHz survey line 5, one meter down the steep bank. Hyperbolic reflections are visible. ... 33

Figure 54: Adjacent survey line of, 0.75 meter down the steep bank. ... 33

Figure 55: 3D visualization with of the first 12 meters of the grid containing the area of a known tunnel entrance. ... 33

Figure 56: 3D visualization of the grid between 15 and 28 meters. ... 33

Figure 57: Three borehole drilled at 5.6 m (left), 24.5 m (middle) and 35.7 m (right) position at various survey lines on the grid (horizontal slice at 0.4-0.45 m/ 5-10 ns depth).Holes reveal that the hyperbolic reflection on the console of the GPR in the field belong to the continues horizon. ... 34

Figure 58: The near overlapping part of the GPR survey line 4 of grid 1 measured with the 500 MHz antenna corresponding to Figure 53. Highlighted in red are reflections that are identified as air-filled tunnels after comparison with the Dipole-Dipole resistivity section. The orange highlighted reflections remain unidentified. ... 35

Figure 59: Dipole-Dipole resistivity section with highlighted in orange interesting anomalies of high resistivity. These are interpret as air-filled cavities and are further compared to the GPR radargram of Figure 58. ... 35

Figure 60: Resistivity section of the Wenner survey. Colour scale is set to correspond to the scale of the Dipole-Dipole section for better comparison. Default scale of the Wenner sections is display in Appendix D. 35

Figure 61: Drill sample profile indicating a lithology (right column) of a 50 cm thick clay layer (green) above peat (brown). (DINOloket 2015) 36

Figure 62: Borehole at location 1 with a 50 cm clay layer present above the peat (black) 36

Figure 63: Borehole at location 2, with 15 cm clay layer 36

Figure 64: Borehole at location 3 near the waterside with assumed tunnels. A 30 cm top clay layer was found. 36

Figure 65: Radargram of 500 MHz antenna survey line at Location 1. Borehole at 4.5 meters discovered an air filled cavity, also indicated by the hyperbolic reflector (red). The velocity is estimated as 0.067 m/ns. Other hyperbolic reflections in green are possible animal tunnels as flags have indicated entrances at the water side. 37

Figure 66: Location 2 500 MHz survey line at position 0 m of the grid, located next to the water with a tree at 2.8 m and a tunnel at 2.2 m. Various reflections from the subsurface are visible. 38

Figure 67: Depth slice at 0.15-0.20 m, grey lines indicate the surveyed line with 0.25 m interval. Line 0.0 m on the vertical axis is the radargram of Figure 66. Highlighted in orange is the muskrat controller's estimation of the tunnel network. At 2.8 m a tree is present and an unidentified signal at 0-0.4 m. 38

Figure 68: Depth slice at 0.60-0.65 m showing strong reflection amplitude at 1.8 till 2.2 m which is interpret as possibly coming from a muskrat tunnel 38

Figure 69: 3D image of the gird shows strong reflections mostly on the waterside and between 0.15 and 0.6 meters deep. The trunk of the tree is identifiable, but the shape of the tunnel is less clear. In the field the GPR failed to show the later unidentified reflections denoted in red. 38

Figure 70: Radargram of 5 m survey line near waterside at location 3, measured with the 500 MHz antenna. No reflections are present due to the thick layer of clay as was discovered by the hand drill. 39

Figure 71: Radargram of 20 m survey line across the meadow at location 3, measured with 500 MHz antenna. Reflections occur between 2.5 and 14.5 meters along the line, possibly due to construction debris filling. After 14.5 meters no reflections from depth due to the top clay layer. Borehole at 6 meter reflection found plastic and shredded wood. 39

List of tables

Table 1: Overview of geophysical methods with their application to near surface cavity detection, sources are found in preceding text. 9

Table 2: Relative permittivity, conductivity and velocity of various materials (Daniels 2004, Di Prinzio et al. 2010) 11

Chapter 1

Introduction

In the Netherlands, water management and flood control are important topics as much of the land is below sea level. For centuries man-made dikes and embankments have protected the reclaimed land from the sea and land-inwards against the flooding of rivers. Since recent the stability of the embankments is being threatened by the burrowing of mammals that live around and within the earthen structures. Native to North America is the muskrat, a rodent fond of water and steep watersides. In the beginning of the twentieth century the animal was brought to Europe and bred for its fur (Heidinga 2006). After being released or escaped, they began to spread rapidly throughout the whole of Europe. In 1941 the first muskrats were found in the Netherlands and at present they are everywhere, except on the islands Texel and Vlieland (Heidinga 2006). Their burrows go into the earthen embankments causing internal erosion and structural integrity losses. In response a national organization was established to manage the population and its activities. The muskrat is not the only animal that poses a threat, bigger in size are the burrows of the coypu and beaver (Figure 1), but both are not as numerous and widespread. In the north close to the border of Germany, the beaver poses a big problem as its tunnels have a diameter of one meter. Muskrat management Zuiderzeeland found a tunnel made by a fox that went all the way through to the other side of the levee. The mouse and the mole dig tunnels below the grass roots, which loosens the soil and causes surface erosion. Even the goose wears the slope down by using the same spot for their landing strip (Muskrat management Zuiderzeeland pers. comm.).

The damages these animals cause make it necessary for the water authorities to continuously monitor the status of the embankments. At present this monitoring implies often only visual inspection of the ground surface and waterside, several times per year. Depending on the nature of the soil invasive damage could go undetected for a long period of time. As consequence there is a high probability that most burrows are not discovered and as such there is an interest for a more thorough approach. Various techniques have raised interest and regularly some are tested. Examples are sensitive sensors placed in the levee measuring all kinds of properties or satellites monitoring the surface subsidence level (Hansje Brinker 2012). Geophysical methods use physical processes and properties of the Earth to characterize the subsurface through image analysis and many variations exist. Ground penetrating radar (GPR) is suited for many near surface investigations, it is used to detected inhomogeneities in river embankments (Biavati et al. 2008) and cavities in a coastal dike (Kang & Hsu 2013). Moreover GPR successfully mapped tunnels of termites (Yang et al. 2009) and moles (Saey et al. 2014). Karst structures though much larger in size than the burrow of the muskrat were detected using airborne electromagnetics (Beard et al. 1994), microgravimetry (Butler 1894) and seismic reflection (Baker et al. 1999).

Most of the research is relatively new and not implemented to the specifics of the muskrat problem in the Netherlands. Their burrows are found in great variety of embankments consisting of different types of soils. Moreover the management organizations demand certain characteristics of the instrument which influences the applicability of the methods (e.g. direct visualization, ease of use and ease of transportation). The objective of this research is to evaluate existing geophysical methods on their functionality in detecting small cavities in embankments caused by local animals in particular the muskrat. Additionally the methods are applied in the field to test their capability to

Figure 1: Mounted beaver (left), muskrat (middle) and coypu (right). Their size in comparison to the muskrat indicates their significant larger burrowing

visualize the spatial extent and depth of the tunnel network in various soils typical to the Netherlands.

This report accounts the progression of the research as it has been performed. First, the scope of the problem caused by the muskrat has been investigated. Various water authorities and muskrat management originations gave insight into their control policy and showed typical sites containing burrows and resulting damage.

Subsequently a literature study has been performed to gain insight in the various existing geophysical approaches and their methodology. The implementation of the methods to the muskrat problem has been evaluated and their advantages and disadvantages judged to determine which method is suitable for further experimentation in the field. Methods with potential in cavity detection which are addressed in the report are ground penetrating radar, electrical resistivity, electromagnetic induction, remote sensing, seismic and infrared tomography. The magnetic and microgravity were found not to be of interest for this research. Field data has been acquired with ground penetrating radar and geo-electric resistivity. These methods are elaborated more in depth to gain understanding of the datasets and subsequent processing steps to achieve a higher signal-to-noise ratio.

The fieldwork took placed on various days during the period between April and June 2015. Locations have been found at the Oostvaardersdijk (sandy subsurface), the Alblasserwaard (clay and peat) and in the Wapenveld area (sand and clay), as denoted in Figure 2. To ground truth interesting anomalies a hand drill has been used to make holes in the ground as to identify their cause.

Finally, the resulting images were analysed and interpreted using various software programs. The geo-electric surveys have resulted in a resistivity section at the Oostvaardersdijk. Cross-sections, horizontal depth slices and three-dimensional images have been created from the ground penetrating radar data of all locations. These multiple perspectives allowed a better understanding of the tunnel network dimensions and connectivity.

Figure 2: Map with the 8 Muskrat management organizations that operate in the Netherlands. The 3 areas at which the measurements of this research have been performed are indicated by stars.

Chapter 2

The muskrat problem

The muskrat is very good in two things: digging and reproducing. The entrances of their burrows are dug below the waterline, sealing it from the threat of predators. Various tunnels then go upwards into the levee and come together in a nesting room where its young are born. A muskrat will have two to three nests per year, with each an average of 6 young (Heidinga 2006). Each litter is born in a separate nest, thus the more it reproduces the more it will dig and the more damage it might cause in the embankment. This chapter discusses the scope of the damage, the management of the Dutch organisations and notes on the problem abroad.

2.1 Damage caused by the muskrat

In 2014, Akkermans (STOWA) filled multiple burrows with PUR-foam and excavated the structure from the surrounding soil, revealing larger dimensions than commonly thought. It was found that the diameters of tunnels were up to 0.25 m and 0.5 m for the nesting rooms. One burrow went 6 m deep into the levee while another was 7 m wide. Overall they were located at 0.3 to 0.8 m below ground surface and the total volume of the tunnel network was up to 300 litres. Figure 3 displays the burrow excavation, revealing its significant size in comparison to the levee. However during this research the tunnels where found to be smaller in size, 0.15 m for the tunnels and 0.35 m for the nesting rooms (Zuiderzeeland pers.comm.). Perhaps the tunnels were larger due to the strength of the foam to expand.

The damage the animals are responsible for is primarily due to their burrowing, which causes internal erosion of the levee and ground surface subsidence (Lammertsma & Niewold 2005). When the water level is high, the outside slope undergoes a high pressure causing water to percolate through the levee. The water flow creates tiny pathways of erosion called the piping phenomenon. In the presence of a burrow this piping is enhanced especially when they are large and continuous across the body of the levee (Chlaib et al. 2014). Subsidence occurs when a tunnel or a nesting room collapses, which can be due to various reasons. In general a muskrat will maintain its lodge, but when it becomes unoccupied it may collapse depending of the type of soil. In clay a burrow can remain undiscovered for years whereas for an unconsolidated soil, like sand, this is less likely. Local subsidence is a danger for agricultural machinery or cattle, as they might step into the cavity. At high water level overtopping is risked when collapse occurs in the crest, small levees can even experience breakthrough due to the tunnelling (Van Hemert & Spoorenberg 2006). Reports have been made on collapsed surface underneath railways and roads as result of the muskrat, causing economic damage (Lammertsma & Niewold 2005). Minor damage results as they eat farm crops and vegetation alongside the water. Additionally the soil volume that is dug out of the embankments into the water has caused higher dredging costs as it clogged the waterway (Lammertsma & Niewold 2005).

Figure 3: Excavating PUR foam filled muskrat burrow with significant size reaching the crest of the embankment (Akkermans 2014)

2.2 Muskrat management

In 1985 increasing concerns on embankment stability led the government to pass a law that puts the responsibility for embankment stability control with the water boards. This means that these boards are responsible for controlling the muskrat population.

At present the well-organized national muskrat management organization has been able to decrease the number of animals caught since 2004 (Figure 4). Nevertheless there is a growing public resistance against the policy; no conclusive evidence has indicated the influence of the policy on the muskrat population or on their damage. Due to the yearly costs of 30 million euros for the management, the question arises whether a more efficient and animal friendly approach is possible at reduced cost. As such the Union of Water Authorities initiated a 3 year scientific experiment to evaluate the current policy (Bos & Tuenter 2007). The experiment has commenced in 2013 and unfortunately no results have yet been released.

At present muskrat controllers are assigned an area they scan for animal traces: damage and subsidence of the embankment, entrances below water level, slantwise chewed reed, floating roots and dung, sand clouds in the water at the beginning of a tunnel, and winter burrows (Muskrat management Vallei en Veluwe pers. comm.). When the traces indicate the presence of a muskrat, the embankment is searched thoroughly for tunnels by inspecting the waterside and pricking the ground (Figure 5). Both lethal and nonlethal catching methods are in use: clamps are placed in entrance and cages on spots with a high catch potential, such as in known migration routes. Both are registered with their coordinates in the national registration program. This allows indication of weak areas as a discovered entrance is defined and registered as damage to the embankment (Vallei en Veluwe pers. comm.).

No geophysical methods are in use by the organizations to assist in detecting burrows. Although there is an interest and innovations are followed, previous experiments with geophysical measurements have been unsatisfactory in both the operation of the equipment and in the results. A frequently mentioned requirement is a user friendly instrument that can be carried lightly, usable on different and difficult terrains, and provides direct results and interpretation. Muskrat management Groot Salland expressed the need for a method that indicates whether a discovered burrow is inhabited or not. As the organisations aim to decrease the population as much as possible, such a method would result in efficient placing of clamps and be less time-consuming. Two organizations have experimented with infrared measurements. Hunze en Aa's performed the measurement in the winter attempting to indicate the warmth of a burrow, but it had no positive outcome. Muskrat management Rivierenland tagged the animals with a tracking device; though a signal was received from below no indication of an entrance was found. At the moment they use a drone with a camera for visual inspection of embankments in inaccessible areas.

As the burrowing influences the embankment's stability the water authorities aim at restoring the levee by excavating the part of the slope that is affected. Most often this only happens when the tunnels are located in a primary embankment. The scope of the affected part is determined by visual inspection and by following the tunnels by puncturing the ground (Zuiderzeeland pers. comm.). Again no geophysical methods are used to assist in determining the size of the burrow. As part of this research it is of interest to determine the effectiveness of geophysical methods in this matter.

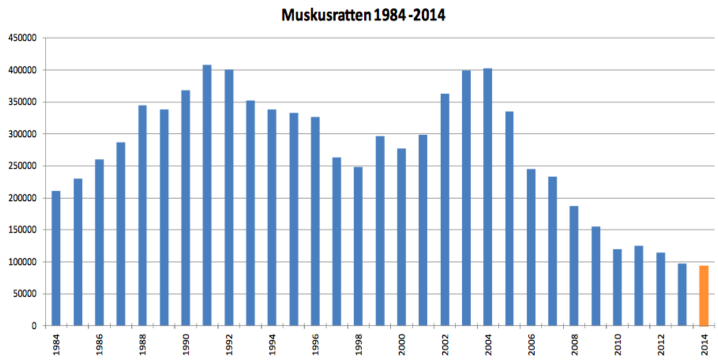

Figure 4: National development of the number of muskrats caught per year. A sharp decrease after 2004 down to 100 000 appears to be stable (Union of Water Authorities 2015)

Figure 5: Muskrat controller inspects the waterside and places clamps indicated by an orange flag (Union of Water Authorities 2014)

2.3 The problem worldwide

Water management is an important topic in the Netherlands and as such the muskrat problem has been taken seriously early in its stage. As previously indicated the effective management techniques and registration system have managed to stabilize the population and reduced the hours of work a muskrat controller needs for the same result. The problem has received significantly less attention abroad as the consequences form less of a thread for national security. However, more and more reports are being made on observed animal activities in earthen dams and levee systems. The lack of natural predators in urbanized and densely populated areas makes human interference necessary to control the population. Efficient management plans and proper maintenance procedures gain interest of organisations globally and a method that contributes to the detection of animal cavities would be beneficial worldwide. Some examples of wildlife nuisance abroad are discussed hereafter.

In the United States the Federal Emergency Management Agency reported 23 main species that are posing a threat to earthen dams among which the beaver, muskrats, gophers, ground squirrels and nutria (Bayoumi & Meguid 2011). Though small in size the squirrel can dig tunnels of enormous length, even completely through a levee and with a record of 33 openings. This network can cause erosion, seepage and subsidence. Additionally after the squirrel has left, the loose soil forms an easy site for other burrowing animals. The beaver builds dams of its own, clogging the waterways and with the potential of flooding. At high water level they dig enormous tunnels into levees and the continuous water flow then causes downstream erosion. Likewise the beaver is a big problem in Bayern in the south of Germany.

China has experienced a widespread outbreak of rodents in agricultural areas in the 1980s. High burrowing activities were found in irrigated farmland, river banks and other earthen structures (Bayoumi & Meguid 2011). In Australia the burrowing activities of the yabby, a native crayfish, leave significant damage to retaining walls of channel, dams and river banks (Bayoumi & Meguid 2011). The porcupine lives in complex burrow systems found throughout the Mediterranean and North Africa. In 2006 the animal was responsible for a major levee failure in the urban area of Sinalunga in Italy (Bayoumi & Meguid 2011).

Chapter 3

A geophysical approach

Geophysical methods aim to characterize the variations in physical parameters of the subsurface. In the case of cavity detection the methods aim to indicate a physical contrast between the cavity and the surrounding rock. The tunnels of the muskrat can be filled with water or air and the surrounding soil consist mostly of clay and sand. In this chapter the problem is approached by various methods.

3.1 Ground penetrating radar

Ground penetrating radar was initially used for glacier ice mapping (Stern 1929) but has since been applied to various other investigations, of which near-surface animal cavity detection (Yang et al. 2009, Chlaib et al. 2014, Saey et al. 2014). The method emits high-frequency electromagnetic waves from a transmitter and detects with a receiver the reflected signal from subsurface features. As the wave travels through the ground it encounters differences in electric permittivity. This contrast causes a reflection of the signal on the boundary between two materials (Daniels 2004). The interpreted travel times from the measured data can be used to create a subsurface image and is displayed in a plot called a radargram. The depth of penetration depends on the frequency of the signal and the physical properties that control the electrical properties of the subsurface, such as the grain size distribution (sorting, clay content), water content, porosity, and the electrical properties of the particles themselves (Mochales et al. 2008). In the presence of conductive materials, such as clay, the signal is attenuated and the penetration depth is minimal (Johnson et al. 2002). Resistive soils, such as dry sands, are best for doing the measurements.

Previous studies have qualified GPR as an efficient tool for mapping shallow objects with high resolution. The method has as great advantage that it is non-invasive and user friendly. Results can be interpreted in real time without any processing making it cost-effective (El-Qady et al. 2005). Its limitations are its poor performance with highly conductive layers and on rough terrain. As such caution should be exercised in selecting the survey site, for levees consist mostly of clay and the waterside can be rough and with high vegetation. In 2014, Kovalenko & Van Isselt conducted a pilot for Fugro using ground penetrating radar to scan for muskrat holes. It was concluded that the burrowing could leave traces detectable by the instrument, but that it is insufficiently distinguished from other anomalies, especially when the levees consist of clay. Nevertheless the method is first of choice for this research.

3.2 Geo-electric methods

Various types of methods are available to determine the electrical properties of the subsurface. They vary in methodology, in applied frequency and in electrical field (Revil et al. 2012). Electrical resistivity tomography (ERT) determines the electrical resistivity by applying a direct current that is transmitted into the ground using current electrodes. This results in a voltage that is measured in the receiver electrodes, giving an indication of the apparent resistivity of the subsurface. The apparent resistivity depends on the mineral and fluid content, porosity, and degree of water saturation in the rock. For the detection of cavities the ERT measurement is applicable due to the high resistivity contrast between the air in the cavity and the surrounding soil. Air has a resistivity that reaches near infinity, while sand is a much lower resistivity and clay has a high conductivity (Putiska et al. 2012).

Various frequently used electrode arrays are available, considering the desired resolution or penetration depth. Both are influenced by changing the spacing between the transmitter and receiver electrodes. For cavities in the shallow subsurface a high resolution is required, while a great depth is not essential. Munk & Sheets (1997) and El-Qady et al. (2005) used the Dipole-Dipole array for similar research applications. The array is sensitive to lateral resistivity changes making it useful for mapping vertical structures such as levees. An array such as the Pole-Dipole gives a deeper depth of penetration, useful when the levees are of greater height, but loses in resolution.

Due to the setup of the electrodes into the ground resistivity methods are suitable for time-lapse measurements, which would be an interesting aspect for investigating the progression of the animal burrowing. A great drawback of the method is that both the setup and the measurement of the survey line are rather time-consuming, as a single measurement can take up hours to complete. In addition the interpretation of the result is not on the spot and requires a high level of expertise. However the method is used for this research to investigate its potential to detect the high resistivity of the air-filled cavity from the surrounding soil and to compare with the GPR results.

3.3 Electromagnetic method

EM is another method that gives an estimation of an electric property namely the conductivity of the subsurface. The method also provides an estimation of the resistivity, as the conductivity is its reciprocal. There is a variety of EM instruments that can be broadly divided into time-domain or frequency-domain methods. However these domains are equivalent and interchangeable through Fourier transformation. With EM induction the fundamental concept is that when a time-varying EM field encounters a conductive object it causes a current to flow within (Daniels et al. 2008). With frequency-domain electromagnetics (FDEM) the transmitter current varies sinusoidally with time at a fixed frequency that is required for a desired depth of penetration, with high frequencies applied for shallow depths. When the generated EM field encounters a conductivity contrast the magnetic field of the EM field induces a current with a direction opposite to the direction of the original field and causes an (secondary) EM field of its own (Daniels et al. 2008). Sensors aim to detect this secondary field as this provides information of subsurface features and anomalies. Transient or time-domain electromagnetics (TDEM) measures the voltage decay over time at a receiver loop caused by the electromotive force (Everett 2013) after the source current in the transmitter loop is switched off. Thus the field is measured in absence of the source current. TDEM can achieve the same as FDEM provided that the data contains sufficient and a relevant number of frequencies. However an advantage of time-domain over is its greater source strength which allows a more favourable depth penetration. An advantage of FD methods is that as the system uses one frequency all other frequencies are noise and can be more easily filtered out, thus it is less subjected to noise.

The above describe methods are simple single transmitter, single antenna systems. The electromagnetic induction method has the advantage that its acquisition is more rapid and easier in surveying than resistivity measurements because no electrodes have to be inserted into the ground. At present electromagnetic instruments can be attached to drones, which would be advantageous for difficult terrain. However it is more subjected to cultural interference as electrical lines and metallic objects (Mochales et al. 2008). For this research EM has not further been investigated for field application.

3.4 Seismic tomography

The velocity of a seismic wave depends on the density and elasticity of the material through which it travels. When a difference in acoustic impedance between two materials is encountered, part of its energy will either reflect off or refract through the interface (Johnson et al. 2002). Through a linear, homogeneous and elastic medium two types of body waves propagate, the compressional P-wave and the shear S-wave. The P-wave propagates in the same direction as the particle motion and at a higher velocity than the S-wave whose particle motion is perpendicular to it propagation direction (Foti et al. 2014). The ratio of the P- and S-wave velocity can be used for interpreting gas or water pockets (Konstantaki et al. 2013). As the S-wave is the back and forth motion of particles in a solid, it does not propagate through an air-filled cavity, whereas the P-wave travels through solids, liquids and gasses. In the pressure free surface of the earth the change in compressibility between soil and the air-filled cavity is so big that the P-waves are reflected form the interface. In the case of an air-filled cavity significantly larger than the wavelength the P and S-wave behave alike. The velocity of the P-wave shows a decrease at a transition to air or another gas and in the case of a transition to a liquid like water the velocity shows an increase. As such a lower ratio V_p/V_s is an indication for the presence of gas, while a higher ratio is an indication for water pockets (Konstantaki et al. 2015). This behaviour of the propagation velocities shows a potential to detect the water or air filled tunnels from the surrounding soil.

The first few meters that are of interest in this research have a severe imaging problem due to dominance of the surface waves. Seismic methods focused on body-waves consider surface waves noise that are to be removed. However recent interest has led to developments to use these surface waves for near-surface characterization (Foti et al. 2014). Surface-wave methods aim to obtain the dispersive characteristics to estimate properties of the soil (Socco & Strobbia 2004). Both the acquisition and processing of such data sets is time-consuming and not realizable in the duration of this research. In addition the interpretation is complicated as the impact of other small heterogeneities increases in the collected data, making the animal cavities less distinguishable.

3.5 Infrared thermography

Infrared measures the variation in temperature at the surface by detecting the infrared radiation of the electromagnetic spectrum. This can be the result of differences in the thermal conductivity and heat capacity of the subsurface (Munk & Sheets 1997), the amount of emitted radiation increases with temperature. Ghafarian Malamiri (2015) used the land surface temperature and soil heat flux to find near-surface layers on the Tibetan plateau. By satellite observation the land surface temperature was measured every hour to model the soil thermal admittance. At present the method measures far too coarse for detecting small sized cavities as the minimal pixel size is an area of 30 by 30 meters (Ghafarian Malamiri pers.comm). Mobile infrared measurements performed in the winter by muskrat management Hunze and Aa's gave no results as no animal presence was detectable.

3.6 Remote sensing

The use of remote sensing is a growing field of research and offers the possibility to integrate geophysical methods on drones. This has as advantage that surveying is not obstructed by inaccessible terrain, as has already been experienced by muskrat management organizations that used drones for visual inspection. However limitations for some methods are due to the requirement of ground coupling and the weight of the instrument.

Another approach is using remote sensing to monitor the variations of the surface level of the levee, as is done by the company Hansje Brinkers. This allows indicating weak parts in embankments as ground subsidence is detected. For this research, application is difficult as only an unoccupied burrow shows a surface level change when the soil is unconsolidated and collapses. Consequently a large amount of burrows cannot be detected using this type remote sensing. In contrast heaps of earth the mole digs up would potentially be discovered as well as winter burrows of the muskrat.

3.7 Carbon dioxide emission

Although not a geophysical method, carbon dioxide measurement have been named by muskrat control organisations and as such it applicability will briefly be addressed. Muskrats can tolerate a high level of carbon dioxide in their blood, enabling them to be submerged for up to 10 to 20 minutes (Feldhamer et al. 2003). This gives them the opportunity to dig their entrances below the water line. The oxygen in muskrat burrow is generally adequate, but especially in the winter months it can build up to high concentrations of 5-7%, followed by a sharp decline by mid-March (Huenecke et al. 1958). Testing the level of carbon dioxide in a discovered entrance could be a method to determining the recent presence of the animals. However it does not give a conclusive indication that the animal is present at the moment and save the winter months the carbon dioxide might be too low to be distinctive. Additionally for application of the method the burrow must have already been found, thus it does not contribution to the detection problem.

3.8 Overview of methods

To summarize the different approaches the overview in Table 2 is created. It is found that most methods do not provide a sufficient resolution to distinguish the tunnel from the surrounding soil. Additionally most methods have too many disadvantages to be applied for the muskrat problem, for example they are too time-consuming or too expensive. Ground penetrating radar and the electrical resistivity method have further been investigated as both are capable in detecting a contrast between the air-filled cavity and the surrounding soil. Furthermore the methods promise to provide a location and depth indication of the cavity. The relative easy measurement setup of the GPR and its possibility to measure a grid with real-time results has given the highest expectations. The ERT method has been chosen for comparison of the results.

Table 1: Overview of geophysical methods with their application to near surface cavity detection, sources are found in preceding text.

Methods	Physical parameter	Conditions	Advantages	Disadvantage
Ground penetrating radar	Electric permittivity	Resistive soil, limited clay or water Ground-coupling	Direct image of subsurface Continuous survey High resolution	Ground coupling Not on rough of high vegetated terrain Attenuation in clay
Geo-electrics	Electrical resistivity	Good ground coupling Resistive soils	Resistivity of air high	Ground coupling Setup labour-intensive Survey time-intensive
Electromagnetics	Conductivity	Conductive soils	Airborne possibility Relative easy and rapid survey	Only bulk volume More subjected to noise
Seismic method	Seismic velocity	Ground coupling	High resolution	Expensive Labour intensive Ground coupling needed
Infrared tomography	Temperature	Satellite observations	Airborne possibility	Minimal penetrating depth To coarse surface area investigation
Remote sensing	Various, altitude changes	Satellite observations	Airborne	Only ground surface analysis
CO_2 emission	CO_2 level	(Recent) inhabited burrow	Possibility to identify animal presence	Burrow must be already known

Chapter 4

Ground penetrating radar

From the literature study in the previous chapter ground penetrating radar has been found to be potentially suited for cavity detection. Before applying the method for field acquisition a more in depth understanding in to the theory is required. This chapter elaborates on the physics behind ground penetrating radar and introduces the equipment that has been used for data acquisition.

4.1 Background theory

Electric permittivity ε, conductivity σ, and magnetic permeability μ are electrical properties of the subsurface. In GPR, ε and σ are the most important properties that influence the propagation of the electromagnetic wave (Jol 2009). A dielectric material is an electrical insulator that does not allow charges to flow freely when placed in an electrical field. Instead of creating a current, charges shift slightly causing a polarization that separates positive and negative charges in opposed direction. This causes an internal field that affects the overall field within the dielectric. The electrical permittivity is a measure of how the electrical field is affected and relates to the applied electric field and the electric displacement or polarization. The ratio of the electric permittivity with the permittivity of vacuum (which is equal to 1) is the relative permittivity $\varepsilon_r = \varepsilon/\varepsilon_0$. The conductivity is the reciprocal of resistivity and describes the ability of a material to conduct an electric current.

When an electromagnetic wave moves through an isotropic medium the direction of propagation is orthogonal to the electric and to the magnetic field (Jol 2009). The wave impedance of an electromagnetic wave is given by Equation 1. The diffusion or propagation of the wave depends on the ratio of energy loss associated with σ or energy storage associated with ε and μ. In the assumption of low-loss $\sigma \ll \omega\varepsilon$ Equation 1 reduces to Equation 2 with further assuming the impedance in free space $Z_0 = \sqrt{\mu_0/\varepsilon_0}$ and $\mu = \mu_0$ (Jol 2009). Equation 3 gives the attenuation where wave energy is converted to heat, which normally gradually increases with frequency. First, this is because water absorbs more energy as frequency increases and secondly due to scattering losses which are extremely frequency dependant (Jol 2009).

$$Z = \sqrt{\frac{j\omega\mu}{\sigma + j\omega\varepsilon}} \tag{1}$$

$$Z = \sqrt{\frac{\mu}{\varepsilon}} = \frac{Z_0}{\sqrt{\varepsilon_r}} \tag{2}$$

$$\alpha = \frac{1}{2}\sigma\sqrt{\frac{\mu}{\varepsilon}} = \frac{Z_0\,\sigma}{2\,\sqrt{\varepsilon_r}} \tag{3}$$

When a radar wave travels through a medium with dielectric properties, charge is stored in the material and impedes the wave from penetrating. In a low dielectric medium, the wave can travel faster. The velocity of the wave through the medium it propagates is given by Equation 4 with c being the velocity in air (Benson 1995). As the wave propagates deeper into the ground it loses part of its energy. Signal attenuation is due to the conductivity of the soil; the higher the ratio of conductivity and permittivity of the material, the faster the wave will dissipate into the ground (Goodman & Piro 2013). Typical values of parameters for some materials are denoted in Table 2.

$$v = \frac{c}{\sqrt{\varepsilon_r}} \tag{4}$$

Table 2: Relative permittivity, conductivity and velocity of various materials (Daniels 2004, Di Prinzio et al. 2010)

Material	ε_r	$\sigma\ (S/m)$	$v\ (m/ns)$
Air	1	0	0.3
Asphalt	2-4	0.01	0.12
Clay	5-40	2-1000	0.06
Concrete	4-10	0.001	0.11
Permafrost	4-8	0.001	0.10
Limestone	7	0.5-2	0.12
Iron	1	1000000	0.0001
Sand (dry)	2-6	0.01	0.15
Sand (wet)	10-30	0.1-1	0.6
Shale	9-16	1-100	0.09
Silt	5-30	1-100	0.07
Water	81	0.01	0.033
Water (salt)	81	4	0.025
Wood	3	0.003	0.17

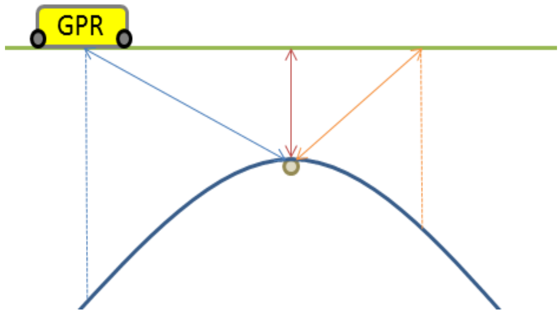

Figure 6: Schematic depiction of hyperbolic response for a small point target, like a tunnel.

At a boundary of a contrast in electric permittivity, part of the incident energy is reflected back and part propagates through the second material, but at a different velocity. This ratio of reflected to incident amplitude is described by the reflection coefficient between the two materials (Equation 5), with θ_1 the angle of incidence and θ_2 the angle of refraction. In a material with zero-conductivity and for vertical incidence the reflection coefficient becomes Equation 6. The reflection coefficient is an indication for the amount of electrical contrast at an interface and not unique for a certain material. When there is no contrast in the subsurface there will be no reflection. The reflection coefficient can also be negative, for instance when the second dielectric is larger. In this case the wave will invert on reflection (Goodman & Piro 2013).

$$R = \frac{Z_2 \cos\theta_1 - Z_1 \cos\theta_2}{Z_2 \cos\theta_1 + Z_1 \cos\theta_2} \tag{5}$$

$$R = \frac{\sqrt{\varepsilon_1} - \sqrt{\varepsilon_2}}{\sqrt{\varepsilon_1} + \sqrt{\varepsilon_2}} \tag{6}$$

The raw result of GPR acquisition is a radargram which displays the data values per unit of time as a function of antenna pair position. When the wave encounters a small point like target, like a rock or the circular cross-section of an animal tunnel, it gives a characteristic hyperbolic response. Figure 6 shows a schematic representation of the space-time curve that represents the arrival time in a simplified medium with constant velocity everywhere between surface and object. The point-like object is detected at other locations than from directly below and as the GPR is moved over the survey line its distance and travel-time changes resulting in a hyperbolic feature. The depth of a reflector d is a function of the velocity (Equation 4) and the two-way travel and can be determined with Equation 7 for a homogeneous and isotropic material (Daniels 2004). In most case the relative permittivity is unknown and the velocity can be determined by measuring the depth of a known target or by performing a common-midpoint measurement.

$$d = \frac{vt}{2} \tag{7}$$

4.2 PulseEKKO PRO

The equipment used for the ground penetrating radar method has been the PulseEKKO PRO from Sensors & Software (Figure 7). Fieldwork has been performed in reflection mode, the most common used survey design that has a fixed antenna geometry which is transported along a survey line to map reflection versus position. During the fieldwork various problem where encountered, some of which made the acquired data unusable. These problems were mostly due to the choice of parameters and some of these will be briefly addressed below.

Figure 7: PulseEKKO Pro 250 MHZ antenna smartcart with GPS system later proved to be inaccurate

Antenna frequencies

The choice of frequencies depends on the desired resolution and depth of penetration. The highest frequency generally gives a higher near-surface resolution, whereas the lowest frequency is preferred when the greater depth of penetration is required (Smith & Jol 1995). As the muskrat burrowing is shallow it has been chosen to measure with the 250, 500, and 1000 MHz antenna.

Antenna orientation

Different orientations of the transmitting and receiving antennas are possible with respect to one another and with respect to the survey direction. The parallel-broadside configuration has ben used for this research as it provides the best coupling between antennas and the most energy in the direction of the survey line, which reduces reflections from targets off to the side of the line (PulseEKKO PRO Manual).

Antenna step size

The step size specifies the distance the antenna pair will be moved each time to collect a new trace along a survey line. The measurements from the first field days were unusable due to incorrectly equalling the antenna step size to the survey line spacing. To properly resolve subsurface targets spatially, the step size has later been set at 1, 2, and 5 centimetres for respectively the 1000, 500, and 250 MHz antenna.

Stacking and skipping traces

Included in the instrument is trace stacking, a way of improving the signal-to-noise ratio when additive random noise is the dominate noise form in the data. At each survey position a trace is collected multiple times, averaged and recorded as the average trace. Noise is usually a random addition to a constant GPR signal and tends to zero out by the square root of the number of stacks, which improves the data quality (Goodman & Piro 2013). The down side is that is slows down the survey measurement, the more stacks the longer it takes to collect data at each survey position. In the field an odometer has been used to trigger the data collection. When walking too fast it triggers too quickly for the system to keep up and the trace is skipped. The system fills the data file as a repeat of the last successfully collected trace. When a large amount of the data is skipped it appears blocky as two or more identical traces are being displayed. This has been experienced in the field with a stacking variable of 32, only when walking very slowly the system could keep up with the triggering pace. The problem has later been resolved by using the DynaQ mode, which dynamically adjusts stacking as the system movement speed varies (PulseEKKO PRO Manual).

GPS measurements

The PulseEKKO PRO included a GPS that allowed measurements up to every trace, but the coordinates proved later to be inaccurate. Instead the GPS of TOPCON Satellite Measuring Systems and Trimble R7/5700 PPK / PPS were used to measure the corner points of the surveyed grids with accuracies up to half a centimetre.

Chapter 5

Electrical resistivity tomography

The second method for further investigation is the electrical resistivity tomography and this chapter will go more in depth on the theory behind the physics. Moreover the instrument used to acquire data in the field is introduced, and certain parameters are addressed.

5.1 Background theory

The resistance R of an object is its opposition to the flow of electrical current and depends on its specific resistivity ρ, size and shape (Equation 8). For a given potential difference U the electrical current I is inversely proportional to the resistance according to Ohms Law (Equation 9). The resistivity quantifies the ability of a material to oppose the flow of an electrical current (Allred et al. 2008). Ground properties such as porosity, pore fluid saturation, ions concentration, clay content and temperature influence the resistivity of the soil. Low values are typical for clay and metallic constituents, whereas hydrocarbons and air have high resistivity values.

In a geo-electric survey electrodes are inserted along a line into the ground and each measurement involves two current electrodes (C_1 and C_2) and two potential electrodes (P_1 and P_2). The geometric factor $K = A/L$ depends on the arrangement of the electrodes and is specific to a certain survey array design.

$$R = \rho \frac{L}{A} \tag{8}$$

$$U = R \cdot I = \frac{\rho \cdot I}{K} \tag{9}$$

$$U = \frac{\rho I}{2\pi} \left[\frac{1}{C_1P_1} + \frac{1}{C_2P_2} - \frac{1}{C_2P_1} - \frac{1}{C_1P_2} \right] \tag{10}$$

The measured potential difference is related to the resistivities of the subsurface and its distribution. Equation 10 gives the potential difference for a homogeneous half-space with C_1P_1 the distance between the current electrode C_1 and the potential electrode P_1. In a heterogonous ground the geometric factor multiplied with the resistance (Equation 9) gives a defined apparent resistivity ρ_a that represents an average of the true resistivity of the subsurface.

Over time five most commonly used arrays have been developed, the Pole-Pole, Pole-Dipole, Dipole-Dipole, Wenner and Schlumberger array (Allred et al. 2008). They differ in the relative configurations between the electrodes, which result in variations in target depth and lateral resolution. When the electrodes are spaced close together the largest fraction of current flows in the uppermost depth and the resistivity resembles the shallow subsurface. In this research one survey line has been performed with two different arrays, the Dipole-Dipole and the Wenner array.

Dipole-Dipole array

The array has its name as both current electrodes are placed at a distance a next to each other and separated at a distance na by potential electrodes also spaced with a (Figure 8). This array uses dipoles, which are closely spaced electrode pairs to measure the curvature of the potential field and is suited to resolve lateral discontinuities and to detect thin lateral resistors in the subsurface by varying n. The apparent resistivity is determined by Equation 11.

$$\rho_a = 2\pi an(n+1)(n+2)\frac{U}{I} \tag{11}$$

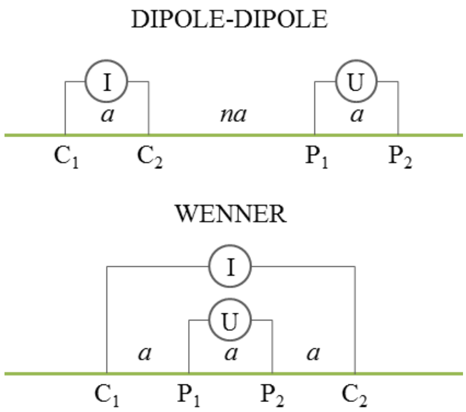

Figure 8: Schematic electrode setup of a Dipole-Dipole and Wenner array

Figure 9: SuperSting setup, with on the left the yellow cables connecting the electrodes with the swift box (middle below) and the SuperSting in the black open box. In the right lower corner the closed black box is the battery

Wenner array

The Wenner array is best used for depth penetration and is used frequently because of its large signal strength. This array consist of four electrodes in line that are separated by an equal interval a. The potential electrodes are place in the middle, while the current electrodes are on the outside (Figure 8). A measurement with a Wenner array is quite time-consuming as the four electrodes are moved along a survey line and is a typical single-channel measurement. The apparent resistivity is determined by Equation 12.

$$\rho_a = 2\pi a \frac{U}{I} \tag{12}$$

5.2 SuperSting R8

Resistivity measurements were performed with the Super Sting R8 IP Earth Resistivity from the manufacturer Advanced Geosciences, Inc. (AGI). The setup included 84 electrodes that were positioned along a line with a spacing of 25 centimetres, thus the resulting cross-section was 20.75 meters long. Fourteen electrodes are connected through one cable, of which in total six were connected on a swift box (Figure 9). Two surveys were measured; a Dipole-Dipole and a Wenner survey, using a survey file created with the software AGI SuperSting Administrator (Version 1.4.0.229). A parameter worth mentioning is the electrode spacing unit, which influences the depth of investigation.

Electrode spacing units

The electrode spacing units define the maximum values for a and na and must be pre-assigned to the SuperSting before measurements. Allowing a larger spacing will result in a greater depth investigated but also a longer measurement time. As the muskrat tunnels are at a depth of 0.5 meters, a desired depth of investigation is about 3 times the electrode spacing (ES). The Dipole-Dipole setup has optimal values for the distance between the transmitter and the receiver, $na = 8$ ES that gives a strong enough signal in most cases. The distance between the poles is set at a maximum $a = 9$ ES for 84 electrodes. However due to wrong implementation the spacings were set at $na = 6$ and $a = 8$, the resulting schematic depiction of the measured points is given in Figure 10. It is observed that the upper 2 ES have a dense collection of data points and that with increasing depth this becomes less dense. The duration for the measurement of this setup was 57 minutes.

For a Wenner setup there is no recommendation as all possible spacings are fine, Figure 11 shows the resulting data points when $a = 9$. Comparing the Dipole-Dipole with the Wenner clearly shows the different approaches as data points using the Wenner array are evenly distributed. In the field the expansion factor for the Wenner was changed to 6 which gave a maximum depth of 3 ES and took 70 minutes to complete, while $a = 9$ results in 5ES depth and takes 105 minutes.

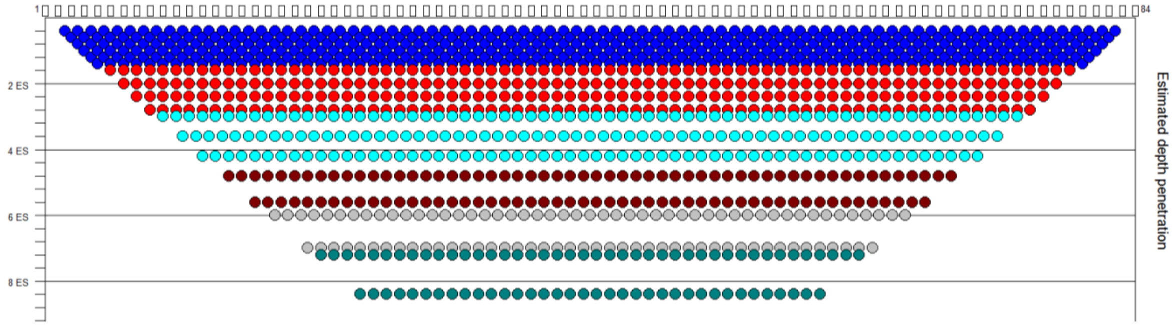

Figure 10: Schematic depiction of measurement points using Dipole-Dipole array with $na = 6$ and $a = 8$, showing many points measured till depth of 2 electrode spacing's (dark blue and red).

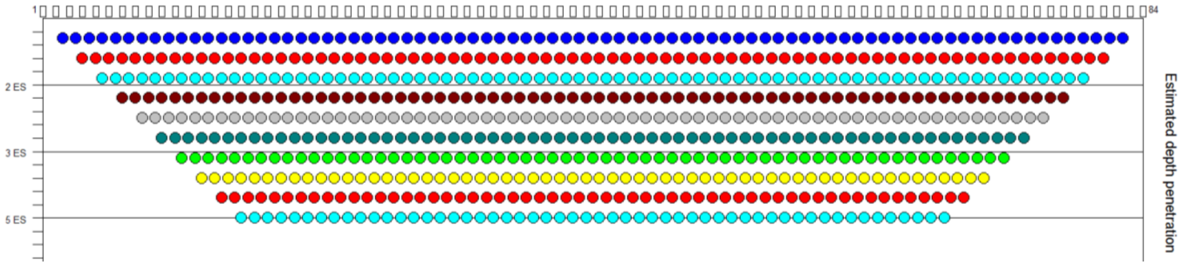

Figure 11: Schematic depiction of measurements points using Wenner array with $a = 9$, showing less measurements points compared to Figure 10. In the field Wenner array was measured with $a = 6$, given a similar section but without the lowest four point line (green, yellow, red and light blue).

Chapter 6

Sites of investigation

As the muskrat problem is widespread and the burrow locations are well documented, sites for investigation were easily found. Muskrats have their habitat not only in levees but in any waterside, even with the slightest slope or the smallest body of water. The locations were selected on their type of soil, the scale of the problem and their accessibility for the equipment. With the ground penetrating radar measurements were carried out in three different regions varying in sand, peat, and clay. An electrical resistivity measurement has been performed only at one location, for comparison with the GPR results. Although not all sites resulted in usable data, they are nevertheless mentioned in this chapter to give more insight in the different embankments found in the Netherlands.

6.1 Oostvaardersdijk, Flevoland

The Oostvaardersdijk is a 30 kilometre primary embankment that protects the province Flevoland against the water of the Markermeer. The Oostvaardersplassen, one of the country's big nature reserves, lie on the levee's inner slope with a 3.7 meters water level difference. The muskrats are protected inside the reserve, making it a breeding paradise (Zuiderzeeland pers. comm.). As a consequence, the Oostvaardersdijk has to deal with major muskrat problems. The importance of the levee and the scope of the problem make it an interesting location for investigation. On the crest of the levee lie a provincial road and a cycling path. The slopes have a thick upper layer of clay, but its bank containing the burrows is mostly of a sandy soil (Appendix A). The bank ends at a ditch filled with water where many entrances are found. The muskrats are persistent at this location with yearly many numbers caught (Zuiderzeeland pers. comm.).

The Oostvaardersdijk has been the first location where measurements were performed and as discussed in Chapter 4 many issues were encountered but overcome. Fieldwork has been performed with GPR on April 10th, 24th and May 27th, and with ERT on June 24th. Weather conditions have been overall dry, as is preferred for GPR, but on May 27th the vegetation has been quite high and disadvantageous for the ground coupling of the radar. Though more grids have been measured, only the following gave usable results:

Section 1: A cross-section of the levee has been measured perpendicular to its stretch, from the side of the cycling path to the waterside where a flag marked an entrance. The section contained the transition from clay to sand and has been measured with all three antennas (Appendix A).

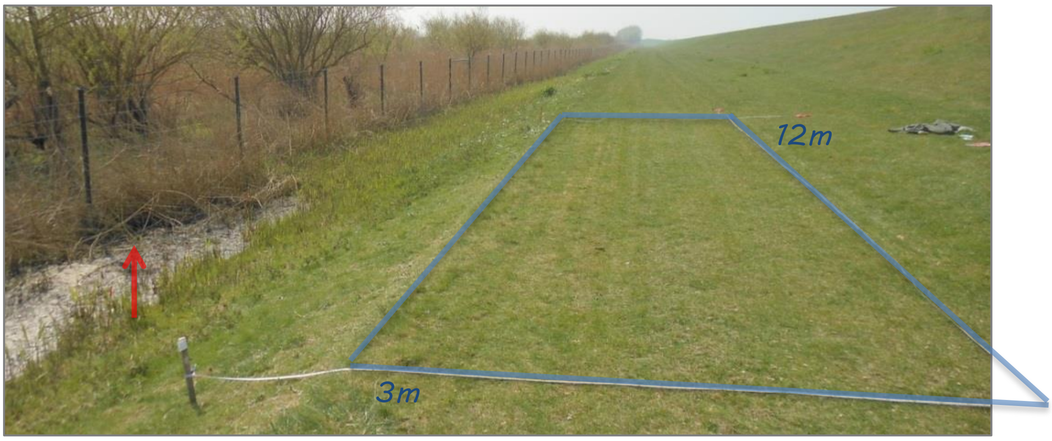

Figure 12: The Oostvaardersdijk with from left to right: water ditch, steep bank, flat bank and steep inside levee slope. In blue the outline of Grid 3 and the red arrow indicates the location the tunnel entrance found by the muskrat controller.

Grid 1: A large grid with dimensions 40 by 1 meters covered the steep bank. Entrances of the burrows were positioned at 5.25 and 35.5 meters along the length of the grid (respectively Entrance 1 and 2 in Figure 13). Measurements were performed with all three antennas.

Grid 2: Similar to Grid 1, but on the flat part of the bank a 40 by 3 meter grid has been measured with all three antennas.

Grid 3: A smaller grid with dimensions 12 by 3 meters on the flat part of the bank (Figure 12). Entrance 2 was now at 3.3 meters length and after 9.5 meters the bank had no water. The grid has been measured with the objective to investigate whether the burrow reached the flat part of the bank and what the effect is of the absence of water. The grid has been measured with all three antennas.

Grid 4: A small 5 by 2 meters grid has been measured with the 500 MHz antenna on the steep part of the bank and centred on Entrance 1. This grid has the objective to investigate the tunnel network as it progressed in the steep slope.

Line 1: The 20.75 meters resistivity section was positioned on the steep bank. Unfortunately due to the high vegetation the marked entrances have not been found. After the field day it has been found with the GPS coordinates that the line failed to include the Entrance 1, however it did reach Entrance 2.

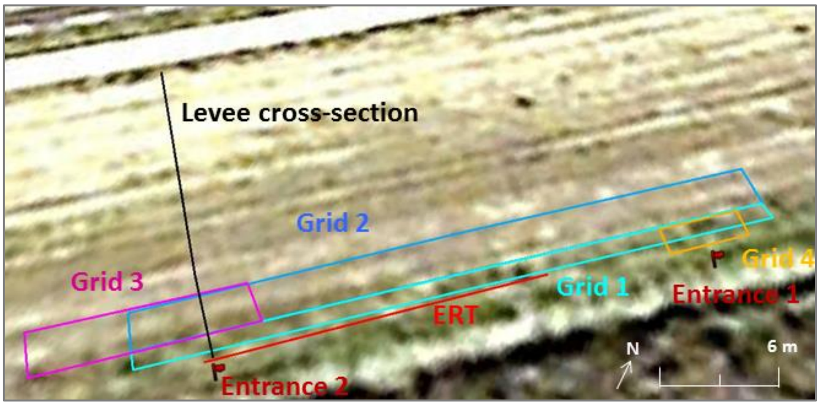

Figure 13: Overview of surveys measured at the Oostvaardersdijk

6.2 Alblasserwaard, South Holland

The Alblasserwaard is a rural area in the South Holland province characterized by agricultural peat lands claimed from the moors during the 10th till 13th century. This polder is bordered by rivers on all sides, with most famously the Lek in the north and includes the Kinderdijk windmills in the west. The grass covered lands are crossed by numerous ditched that form an ideal habitat for the muskrats. To determine the ability of the GPR to detect the burrows with a subsurface of peat, various locations in the area have been investigated. The locations have been selected by the local muskrat controllers of the Rivierenland district. On the 28th of May ground penetrating radar fieldwork was conducted with rainy weather conditions in the morning.

Location 1: The first location was in a polder close to the river Lek with a concrete road near the waterside for easy access (Figure 14). With over fourteen flags indicating entrances in a waterside of 20 meters, the site seemed perfect for investigation. However after a test survey, barely any signal was received. A borehole with a hand drill indicated at 20 cm depth a 50 cm thick clay layer. Moreover the terrain was rough, with irregular humps making it difficult to smoothly push the equipment without losing ground contact. Thereby only one survey line of 14 meters was performed with all three frequencies, to investigate the influence of the clay layer.

Figure 14: The narrow first location at Alblasserwaard with entrances at the waterside indicated by the orange flags. The white line denotes the 14 m surveyed line ending at the GPS.

Figure 15: Location 2 on a mound with entrances found around the tree. Flags are displaying the corner point of the 1.25 by 4 m grid measured with the 500 and 1000 MHz antenna. The high grass had to be mowed first to make it accessible for the GPR equipment.

Figure 16: Low vegetation at Location 3. The outer flags in the water are preventive clamps; the 3 middle flags (positioned in the grass) indicate the actual entrances

Figure 17: The grass field of Location 4 at Wapenveld with a muskrat entrance highlighted in red. The subsurface contained a too thick layer of clay

Location 2: The second location was on an elevated road higher above the water level (Figure 15). It was a remote location vegetated with high grass, which had first to be mowed with a scythe to make it accessible for the radar equipment. At the waterside three entrances have been found around the tree. A small grid of 1.25 m wide and 4 m long was measured with the 500 and 1000 MHz antenna.

Location 3: A site with easy access and low vegetation was sought after and resulted in the third location with 3 entrances (Figure 16). Unfortunately a 5 m test line near the water with the 500 MHz antenna showed again no reflections due to too much clay. Hence no grid was measured here, however out of curiosity a 20 m line across the meadow gave half-way surprisingly many reflections.

6.3 Wapenveld, Gelderland

The village Wapenveld is situated between the forest and heathlands of the Veluwe on the west and the lower laying riverbanks of the IJssel in the east. The sandy soil of the heath was thought to be a perfect location for the ground penetrating radar. However the local muskrat controller showed that in the Veluwe muskrats are seldom found, in contrast to the river plains where they are numerous. Unfortunately a top layer of clay is dominant in the plains and the vegetation was high on the day of the fieldwork. As consequence most of the sites have either been unsuitable due to the soil or inaccessible due to the vegetation. On June 10th only two locations have been investigated.

Location 4: In the polder of the IJssel this grass field had a narrow ditch and barely any height above the water level, nevertheless a muskrat had dug an entrance (Figure 17). As the location had a thick layer of clay, only a small grid with dimension 3 by 5 meters was measured with the 500 MHz antenna.

Location 5: Situated next to a brook this embankment of sand was quite high and went down steep to the water (Figure 18). A muskrat burrow was found here a long time ago and it was unlikely it would go up as high for the radar to detect. As the soil was of sand it was suitable to create an artificial tunnel to test the GPR response. This 15 cm diameter tunnel was positioned at 2.7 m along a 5 m survey line at a depth of 20 cm and went 1 m in the slope of the embankment. The survey line was measured with all three antennas twice, with one measurement the metallic hand drill was place inside the tunnel.

Figure 18: Steep embankment at Location 5 where a test hole (position denoted with a red circle) has been created to investigated response of the GPR

6.4 Remarks on sites of investigation

During the days in the field many different locations have been visited in various areas in the country, some of which have not been displayed in this chapter. As the objective of this research is to investigate the applicability of geophysical methods on the muskrat problem in the Netherlands some remarks can already be made.

Muskrat controllers throughout the country investigate thousands of kilometres of waterways with a great variety in soil and structure. To successfully contribute to the problem a method must be applicable to at least a significant majority of embankments. It has been found that some embankments are either too steep for comfortable GPR surveying (Figure 18), too tortuous or the terrain was too rough for proper ground coupling of the antennas. Clay forms another problem for the ground radar and is a dominant soil type in the Netherlands, especially in agricultural areas and as a top layer against erosion in levees. Another crucial factor is the vegetation of embankment. In the Netherlands stimulating the biodiversity gains importance and as such water authorities are subjected to create nature friendly watersides. This means that in a strip close to the water vegetation is not mowed and allowed to grow wild. As the tunnels are especially in this part applying GPR and ERT becomes increasingly difficult as was experienced in the fieldwork during May and June, also the months of muskrat breeding season. The GPR antennas require close ground contact, which is near impossible with vegetation over a meter and for ERT placing the electrodes becomes a nuisance in the present of nettles.

Apart from their capability to detect muskrat tunnels the methods must also be judged on their practical applicability. When the methods become more time-consuming the organisation will be forced to employ more people to still be able to investigate the entire amount of waterways. And the question arises whether that is desirable as the costs of the management will also increase.

Chapter 7

Data processing

Raw geophysical data undergoes various processing steps to decrease the amount of noise contained in the data and increase the resolution of the image. Using physical laws and statistics a higher signal-to-noise ratio can be achieved, which improves the image and makes its interpretation more accurate. The GPR and ERT data have been processed using software created by the manufacturers of the instruments. This chapter discusses some relevant processing steps and shows their influence on the subsurface image.

7.1 Processing the GPR signal

The data was processed using the software EKKO_Project created by Sensors & Software GPR. Additionally a MATLAB program matGPR (Tzanis 2010) contributed to familiarizing with the raw data and various processing steps. The 3D data visualization program Voxler developed by Golden Software Inc. was used to create 3D images of the data, allowing a better insight on the tunnel connectivity.

7.1.1 Basic handling in EKKO_Project

The EKKO_Project software has a variety of processing possibilities but only a few basic steps have been applied on the data of this research, giving sufficient images suitable for straightforward interpretation. The very first step applied on the data is moving the start time of the pulse with a certain value to make the first arrival of the signal corresponding to zero-time. Additional steps applied to the 250 MHz radargram of Grid 3 line 7 are discussed and visualized in Figure 20 to Figure 24. It is noted that as the raw signal barely has strength in amplitude these Figures already have a gain applied to better show the effect of the processing step.

Dewow filtering

A GPR trace contains various unwanted frequencies among which the wow, a slowly decaying or increasing low frequency component. This noise may be induced on the traces by the transmitting signal due to the proximity of transmitter and receiver (Jol 2009). By applying dewow, the mean is calculated, within a window of width equal to the pulsewidth, for each value of each trace and subtracted from a central point. Figure 20 shows the radargram without dewow applied, where noise dominates the deeper part, and Figure 21 shows the improved image.

Background removal

Horizontal bands across the radargram are a much observed noise in the acquired data. This is the result of a constant infiltrating noise during the recording of the raw signal. The background filter calculates the average pulse across the entire radargram and subtracts this average then from each individual recorded pulse (Goodman & Piro 2013). Figure 21 shows horizontal bands at 35, 50 and 60 ns, implying phantom reflections which disappear with background removal in Figure 22. Not only noise bands are affected by the filter but also horizontal reflections continuous across the radargram. Normally this is not desired but in the case of cavity detection this is advantageous as hyperbolic reflections are unaffected and become more distinct. The improved radargram shows also enhanced reflections in the deeper part.

Applying a gain function

Various methods are available to restore the amplitude of the signal as it attenuates with increasing depth. Figure 19 shows trace 80 of line 7 which is at 8.4 m position with various gains applied. The black line indicates the raw signal and shows its rather rapid attenuation. The applied gains are indicated by a blue line and the resulting signal is shown in red. In the lower half of Figure 19A the wow is still present and the effect of the background removal is seen when comparing B and C.

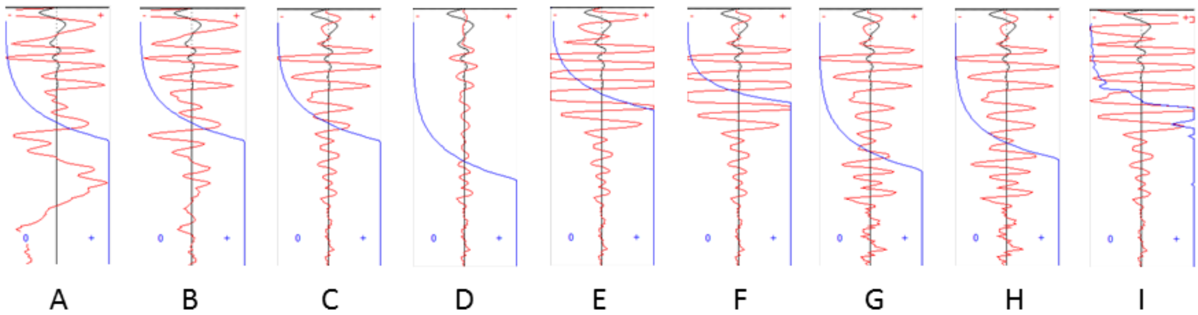

Figure 19: Line 7, trace 80 of Grid 3 measured with the 250 MHz antenna displaying various processing steps applied, black line indicates raw data; red line processed data; blue line indicates applied gain. Below processing steps are denoted with att=attenuation, start=start gain, max=maximum gain, window=window width:

A)	*SEG2 (automatic parameters: att=11.35, start=4.49, max=477)*	*(see Figure 20)*
B)	*SEG2 (att=11.35, start=4.49, max=477) + dewow*	*(see Figure 21)*
C)	*SEG2 (att=11.35, start=4.49, max=477) + dewow + background removal*	*(see Figure 22)*
D)	*SEG2 (att=11.35, start=1, max=477) + dewow + background removal*	*(see Appendix B)*
E)	*SEG2 (att=11.35, start=15, max=477) + dewow + background removal*	*(see Appendix B)*
F)	*SEG2 (att=20, start=4.49, max=477) + dewow + background removal*	*(see Appendix B)*
G)	*SEG2 (att=11.35, start=4.49, max=1500) + dewow + background removal*	*(see Appendix B)*
H)	*SEG2 (att=13, start=4, max=1500) + dewow + background removal*	*(see Figure 23)*
I)	*AGC (window=1.5, max=500) + dewow + background removal*	*(see Figure 24)*

The EKKO_Project software recommends a Spreading Exponential Calibrated Compensation (SEC2) which applies an exponentially increasing gain as a function of depth. Parameters that shape the gain are the attenuation, start gain and maximum gain (EKKO_Project Manual 2015). The attenuation (given in dB/m) determines the steepness of the ramp, increasing this value will give a steeper slope (Figure 19F). The start gain specifies the initial gain value at zero depth and higher values will result in steeper ramps (Figure 19C, D and E). The maximum gain sets the value after which the gain will not increase further; this is used to avoid excessive gain for deeper depth (Figure 19G). The values of the parameters in Figure 19C have been proposed by the software and resulted in the radargram of Figure 22, however the user can play with the values to optimize the image. Using the gain of Figure 19H the radargram of Figure 23 was acquired, now the reflections at depth greater than 30 ns have become stronger. Increasing reflections from the deeper part of the radargram can be valuable when there is an indication that the burrows are located that deep. However this was not the case with all surveys and an increased gain was not desired here as it also increases the noise.

The Automatic Gain Control attempts to equalize the signal by applying a variable gain inversely proportional to the signal strength (EKKO_Project Manual 2015). This has as a downside that the relative signal amplitudes between reflectors are not preserved. Variables that shape the applied gain are the window width or the time duration of the signal used to determine the signal strength and the maximum gain. Figure 19I shows the gain applied on the signal and the resulting radargram is display in Figure 24. As the targets of investigation are small air filled cavities, these relative differences are important when for instance comparing to a rock or a metallic object. As such it was chosen to amplify the data of this research with a SEC2 gain as it gives a more realistic image.

Horizontal time and depth slices

The two dimensional representation of a cross-section is more difficult to interpreted when a grid is measured. The multiple lines adjacent to each other in a grid can be interpolated as a 3D block and presented as a horizontal slice in either depth or time intervals. A slice shows the average amplitude strength of the chosen interval, thus for a realistic representation the chosen interval must be small. Spatial correlations and targets are better interpreted and differentiated from areas of no interest as for example the tunnels of the muskrat tend to produce linear structures.

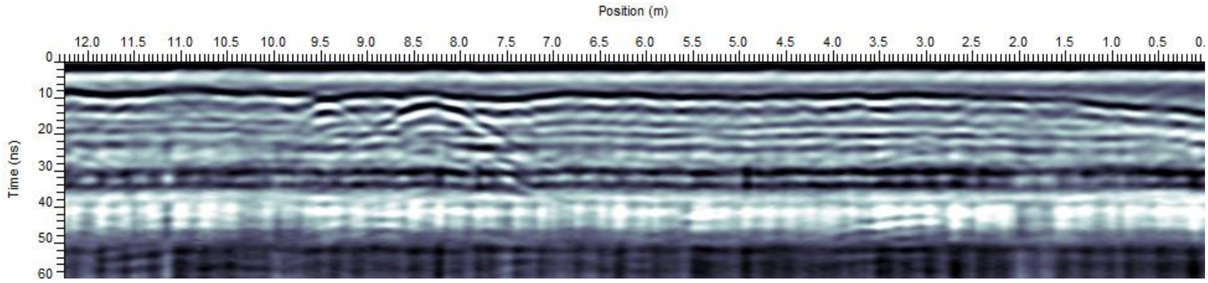

Figure 20: Radargram corresponding to Figure 19A with SEG2 gain applied, automatic parameters recommended by EKKO_Project. Wow dominates in deeper part.

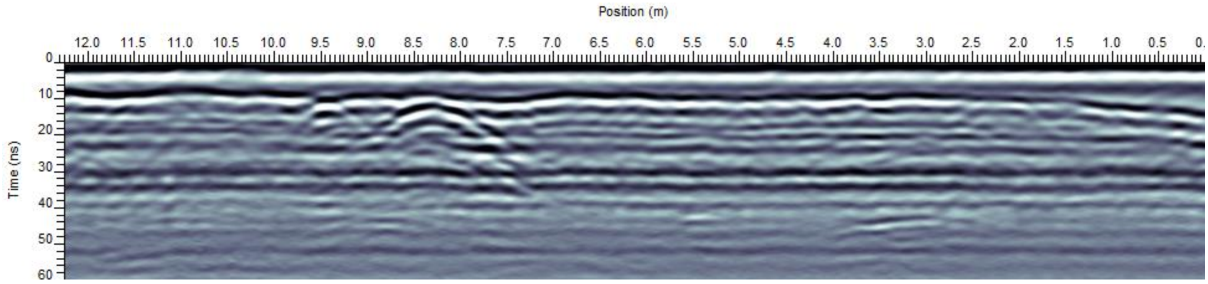

Figure 21: Radargram corresponding to Figure 19B with SEG2 and dewow applied. Horizontal noise band is still present at around 30 ns, indicating a phantom reflection.

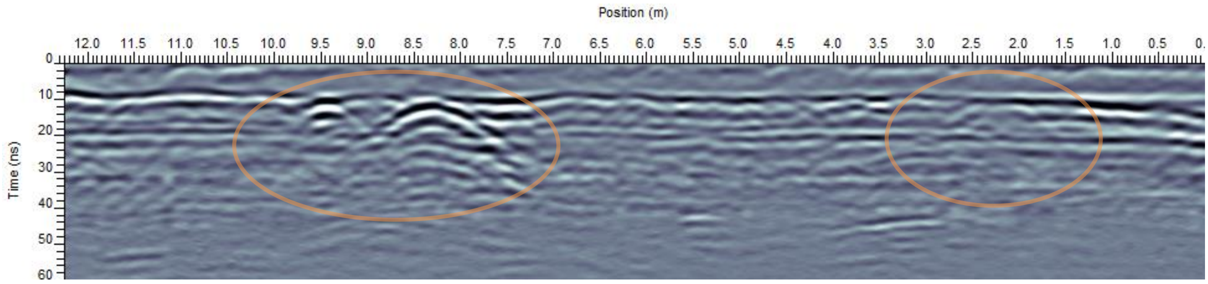

Figure 22: Radargram corresponding to Figure 19C with SEG2, dewow and background removal applied. Image contains less noise, the horizontal layer at 10 ns and the hyperbolic reflections (highlighted in orange) are more distinct.

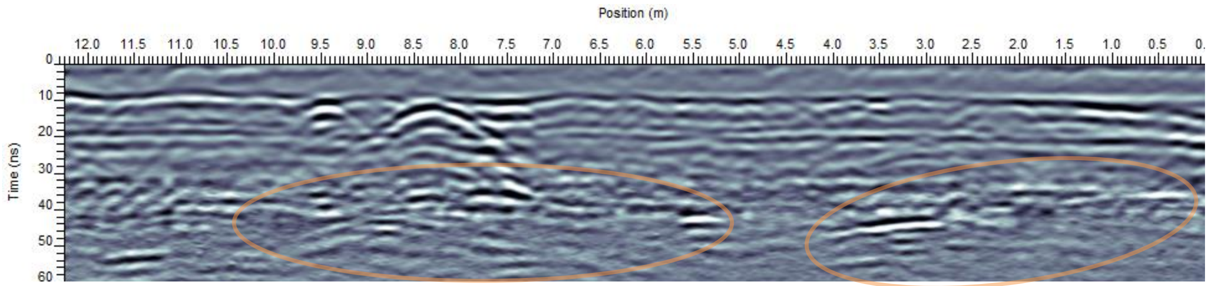

Figure 23: Radargram corresponding to Figure 19H with SEG2 gain applied, parameters are chosen by the user to increase strength from signals at depth greater than 30 ns (highlighted in orange).

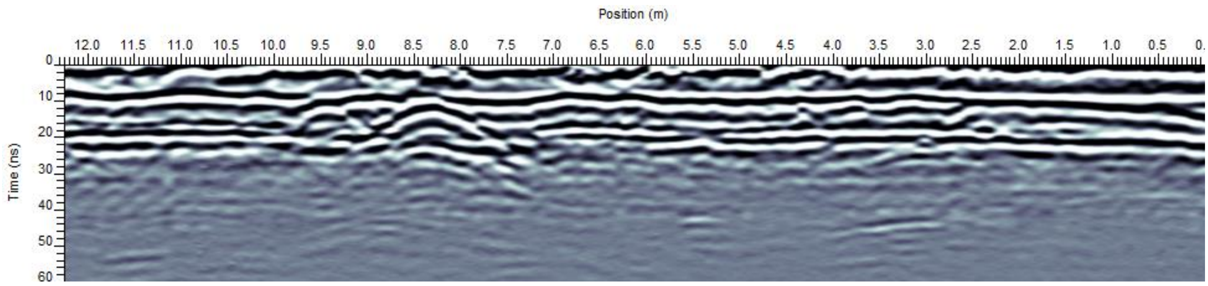

Figure 24: Radargram corresponding to Figure 19I with AGC, dewow and background removal applied. Relative signal amplitude is lost, especially in the upper 20 ns. The reflections are less distinct with AGC than with SEG2 applied.

The colour scale used for the horizontal slices differs from the radargram, as instead of a black to white scale it is in displayed in a rainbow scale (Figure 25). With the radargram negative amplitudes of the signal are indicated by the black side of the scale, whereas a positive signal goes towards white. For the horizontal slices the absolute value of the amplitude strength is used. As such a strong white or black signal on the radargram transform on to a red signal, while a small absolute amplitude strength converts to the blue side.

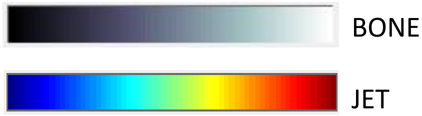

Figure 25: Colour bars user for radargrams (bone) and slices (jet)

7.1.2 3D imaging in Voxler

Grid surveyed data can be exported from EKKO_Project for processing and visualization with other software programmes such as Golden Software's Voxler. This data is exported as the 3D location of each point within the grid (X, Y, Z) and the average signal strength or amplitude at that point. The dimensions X and Y are controlled by a preferred value of the slice resolution, in case of the muskrats tunnel this was set at 2 cm, the minimum value possible in the program. The Z dimension is controlled by the thickness of the depth slice, which was set either at 0.5 cm or 1 cm. Such small dimensions are necessary as the tunnels themselves are often just 15 cm wide, however with the largest grid (Grid 1 and 2) of this research the size of the 3D file became too large for Voxler to operate with and a coarser resolution was required.

Voxler provides various viewing option, one of which is the scatter plot and is displayed in Figure 26. Tunnel connectivity can be analysed in 3D by creating an isosurface, a value corresponding to the desired amplitude strength is persevered while all values greater and smaller are left out. These results will be addressed in the subsequent chapter.

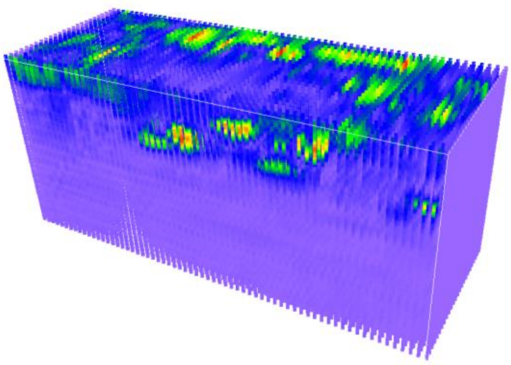

Figure 26: Scatter plot of GPR data made by Voxler of Grid 4 on the steep bank of the Oostvaardersdijk

7.2 ERT processing

The data was processed using EarthImager 2D (Version 2.4.0) developed by Advanced Geosciences, Inc. The program displays the measured apparent resistivity and allows user-friendly inversion of the 2D sections with enough options for a more advanced processing. Inverse modelling aims at determining subsurface properties using observed data. Creating a data model with predefined parameters is forward modelling and provides useful insight into the nature of a geophysical problem. In EarthImager 2D, the inverted section is forward modelled for evaluating the calculated with measured apparent resistivity.

7.2.1 Inverse modelling

The objective of this inversion is to find a resistivity model whose apparent resistivity, calculated by the forward model, best fits the measured data. Figure 27 displays sections of the Dipole-Dipole survey as result of various processing parameters discussed hereafter. For the Wenner section similar steps have been applied (Appendix C), however they are not addressed separately here. The upper section displays the measured apparent resistivity, the bottom section is the resistivity after inversion and the middle section shows the calculated apparent resistivity after forward modelling. The maximum root mean square (RMS) error characterizes the goodness of the fit and can be seen as a threshold for accepting subsurface values.

Root mean square error

The RMS error is a frequently used measure for the difference between the measured data d^{Meas} and the data predicted d^{Pred} by the forward model, defined by Equation 13 with N the total number of data points (EarthImager 2D Manual 2009). The equation shows that the error depends on the number of bad points in the data and on how bad each bad data point is.

$$RMS = \sqrt{\frac{\sum_{i=1}^{N}\left(\frac{d_i^{Pred} - d_i^{Meas}}{d_i^{Meas}}\right)^2}{N}} \times 100\% \tag{13}$$

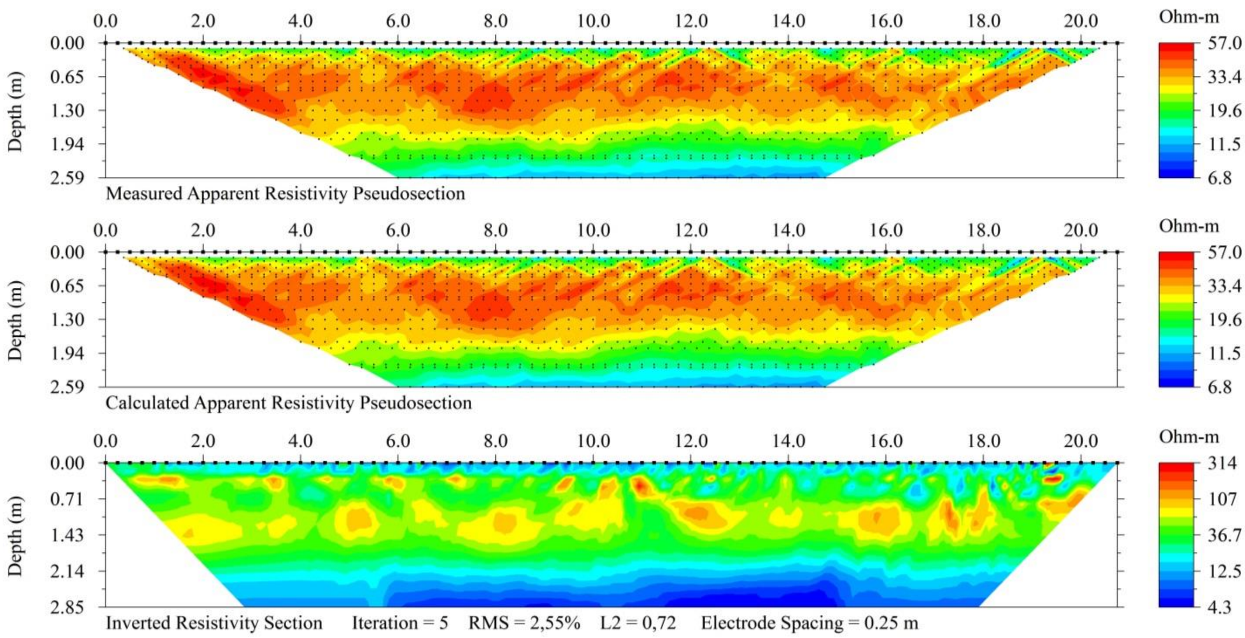

Figure 27: Resistivity sections of Dipole-Dipole survey processed with EarthImager 2D. Top section depicts the measured apparent resistivity, middle section the calculated apparent resistivity from the bottom section. Parameters for inversion were a maximum RMS of 3% and a smoothing and damping factor of 10. Forward modelling was performed with the finite element method, using a Cholesky Decomposition forward solver equation and a mixed boundary condition. The upper two sections form a near exact resemblance and as such these parameters were chosen to fit best.

A large RMS error can be the result of noise in the data, errors in numerical modelling or poor inversion settings. When the forward model has a higher RMS error than acceptable the program repeats the inversion to obtain the desired value, it performs a so called iteration. The number of iterations also provides information on the quality of the data. When the RMS error decrease little or increases from iteration to iteration the inversions should be terminated. The software suggests a maximum RMS error of 3%. Figure 28 shows that the RMS error converges when allowing more iteration. After 5 iterations a RMS error of 2.55% has been achieved and after 7 a value of 1.57%, more iterations did not manage to significantly decrease the error as after 10 the value was 1.40%. The RMS error is not an indication of the percentage of bad data points but provides an average data misfit over all data points. It does not define the error of the model itself, however a low value is an indication that overall the predicted data points fit well to the measured points and the model is plausible. Thus the choice of 3% as maximum value for the RMS error appears to be sufficient as this gives the minimal number of iterations for a similar accuracy.

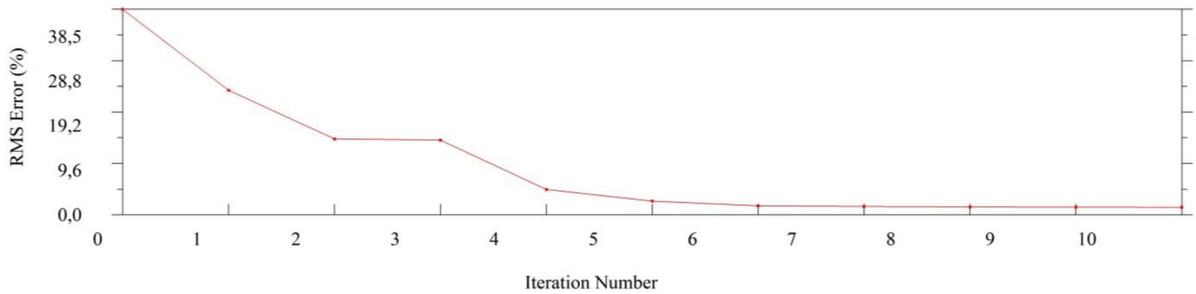

Figure 28: Convergence curve of resistivity inversion similar to Figure 27 but with no maximum value for the RMS error assigned. The graph shows that an acceptable RMS error is achieved after 5 iterations.

Smoothing and damping factor

There are additional steps that can stabilize the inversion by considering prior information in an inversion problem. Damping aims at minimalizing the difference between the estimated and reference model parameters, while smoothing imposes constraints on structural features (EarthImager 2D Manual 2009). A small smoothness factor produces a relatively rough model, while a large smoothness factor will produces a relative smooth model. Various values have been tested on the measured data, and a best result has been found to be 10. As suggested by the program the same value is set for the damping factor.

7.2.2 Forward modelling

Various methods for forward modelling exist and the EarthImager 2D allows two, the fine element method and finite difference method. The finite difference method is faster but the finite element produces a more accurate forward modelling solution.

Forward solver equation

The program offers two options, the Cholesky decomposition or the conjugate gradient forward solver. The first is much faster when using more than 20 electrodes, and as such was preferred for the data. The conjugate gradient was terminated when after 3 minutes and 25 iterations the RMS error was still above 26%, while the Cholesky needed 5 iterations in 23 seconds to achieve an RMS error 2.55% (Figure 27). An advantage of the conjugate gradient solver is it much less use of memory space.

Boundary conditions

The ground surface is always imposed by the Neumann boundary condition, while the left, right and bottom boundaries have the options Dirichlet or mixed. Mixed boundary conditions produce a more accurate forward solution, but in the program the effects have not been recognizable.

7.2.3 Data misfit analysis

At the end of inverse and forward modelling, the misfit of the data and individual data points are analysed. The relative data misfit is defined by Equation 14 as the ratio of the difference between the calculated and measured data to the measured data (EarthImager 2D Manual 2009). For the Dipole-Dipole section the misfit is shown with a scatter plot (Figure 29) and with a histogram (Figure 30). Data misfit values up to ±14% are found mostly on the right of the section. Large single erroneous data points lead to a larger RMS error and should be removed. In general, a threshold at 50% relative data misfit is advised by the software. As the Dipole-Dipole and Wenner (also ±14%) sections contained values significantly lower no data points have been removed.

$$relative\ data\ misfit = \frac{d^{Pred} - d^{Meas}}{d^{Meas}} \times 100\% \qquad (14)$$

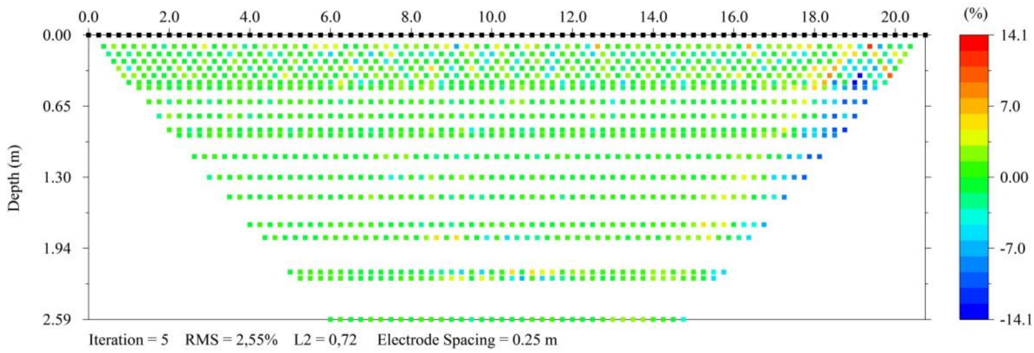

Figure 29: Data misfit scatter plot, showing high deviations mostly at data points on the right of the section.

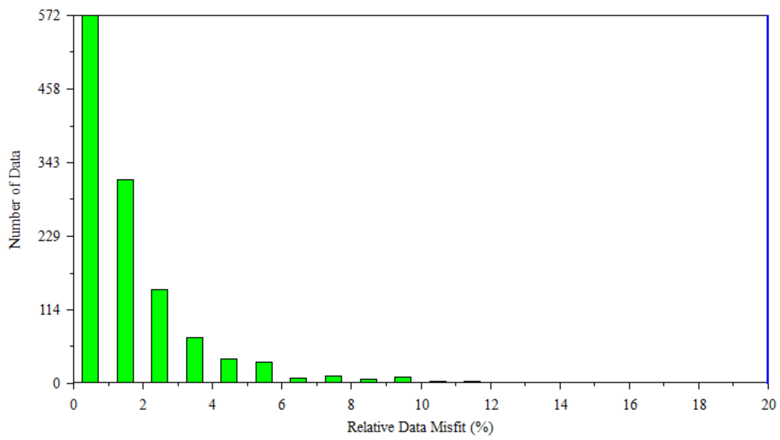

Figure 30: Data misfit histogram for removal of poorly-fit data. However in this case no points have been removed as the misfit values are acceptable.

Chapter 8

Results and interpretations

This chapter aims at interpretation of the acquired data, but before elaborating on the results a short note must be made on the image visible on the GPR console in the field. It was inadequate in showing a detailed image especially with small reflections that elsewise appeared on the computer software. Consequently the hand drill brought to the field to ground truth anomalies, was not applied on most hyperbolic reflections. For the interpretation this is unfortunate as some anomalies and reflections remain unidentified and assumptions now lack evidence. At the end of the chapter the results and interpretations are discussed.

8.1 Artificial tunnel at Wapenveld

Close to the end of the research, the artificial tunnel gave an interesting insight in the ability of the ground radar to detect a near surface cavity. All three antennas have been tested on the 15 cm wide hole created at 20 cm depth, 1 m into the slope of the steep and sandy embankment (Figure 31). Additionally the metallic pole of the hand drill has been placed inside to investigate its effect on the signal. In retrospect, it would have been preferred to begin with such an experiment to better understand the GPR results of the Oostvaardersdijk en the Alblasserwaard.

8.1.1 250 MHz antenna

On arrival a first test line has been conducted with the 250 MHz antenna to determine whether the soil of the site is suitable for the radar (Figure 32). This is the case as many reflections have been received from the sandy subsurface. Figure 33 shows the 5 m survey line with the artificial tunnel at 2.7 m position, while Figure 34 shows the response when the hole contained the metallic pole. The Figures manage to visualize a difference (in orange highlighted area), however in the field the image on the console was too coarse. The air filled tunnel shows a small hyperbole at 10 ns depth, this

↓ Figure 32: Test line measured with the 250 MHz antenna shows no clear reflection within the orange highlighted area. The red box denotes survey line of Figure 33 and Figure 34

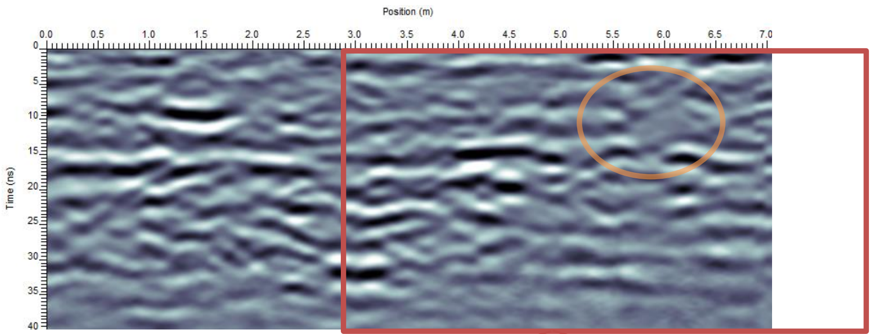

Figure 31: Artificial tunnel in sandy soil at 20 cm depth.

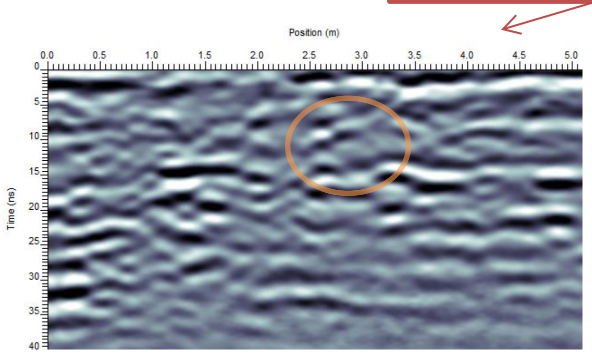

Figure 33: Survey line with artificial tunnel at 20 cm depth positioned at 2.7 m along the line. The orange circle indicates a weak hyperbolic reflection.

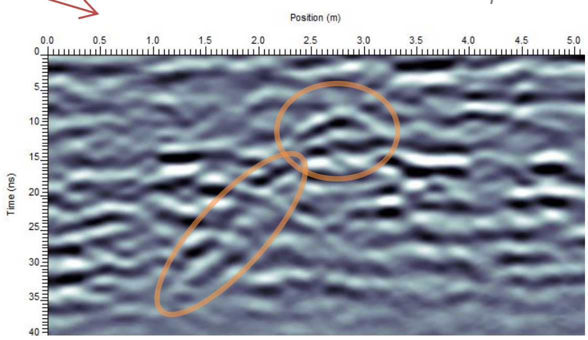

Figure 34: Metallic hand drill in the tunnel gives a strong distinct hyperbolic reflection with a left leg

reflection is weak and without prior knowledge would probably not have been identified as coming from the tunnel. The metal pole does create a strong hyperbolic reflection, with even a strong left leg (Figure 34).

8.1.2 500 MHz antenna

The radargram acquired with the 500 MHz antenna (Figure 36) shows a weak hyperbolic reflection coming from the air filled tunnel at 10 ns depth. Again it would have been difficult to distinguish it from the many other reflections when the presence is unknown. Strong is the hyperbole in Figure 37 as response of the two metal poles placed inside the hole.

When comparing the results of the 500 MHz with the 250 MHz antenna, the first gives a much better resolution of the shallowest 24 ns. In the 250 MHz radargram a lot of detail is lost and the reflections are more smoothened out. Knowing that the tunnel is located at a depth of 20 cm top and 35 cm at its bottom, the velocity of the subsurface is determined with Equation 5 to be 0.075 m/ns.

Polarity change

The hyperbolic reflections show a difference in polarity. The air-filled cavity of Figure 36 shows a weak black-white-black reflection, while the metal poles cause the strong white-black-white reflection of Figure 37. This is also seen on amplitude of the signal at the location of the tunnel (Figure 35). The relative permittivity of air is 1, which is smaller than most other materials. From Equation 5 is derived that going from a soil to air means that $\varepsilon_1 > \varepsilon_2$ and $Z_1 < Z_2$ thus $R > 0$, which gives a positive peak. In the case of the metal pole the conductivity is much higher $\sigma_2 \gg \sigma_1$ so that $Z_1 > Z_2$ and thus $R < 0$ will give a negative peak. A negative peak is also the case when going from a smaller to a higher relative permittivity, as is the case from a soil to water (81). Hence the reflection type is useful for the discrimination of an air-filled tunnel from other objects.

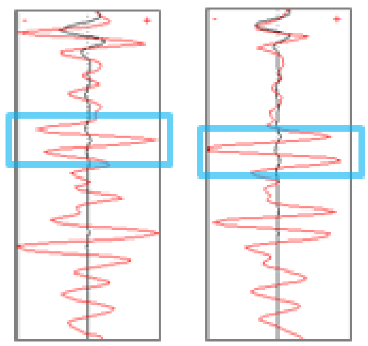

Figure 35: Amplitude of signal at tunnel, positive peak when air-filled (left), negative peak when containing metal (right)

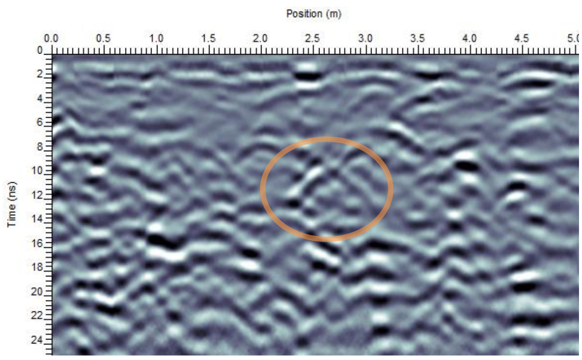

Figure 36: 500 MHz radargram showing weak reflection around 10 ns depth of tunnel without metal pole.

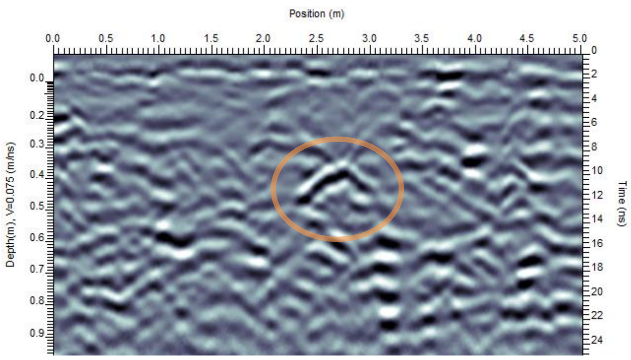

Figure 37: Two metal poles placed in the tunnel gives a strong hyperbolic reflection. Left axis with known depth of the tunnel estimate a 0.075 m/ns velocity

8.1.3 1000 MHz antenna

In the field the 1000 MHz antenna showed barely any reflections, which was also the case with the software on the computer. The images show too many scattering objects in the ground, making it difficult to see the reflection from the air-filled tunnel. The antenna was not even capable to distinguish the metal pipe in the artificial hole, causing Figure 38 and Figure 39 to be near identical. Moreover, the antenna easily has a poor ground contact on an uneven surface creating vertical bands of noisy data (highlighted blue in Figure 38).

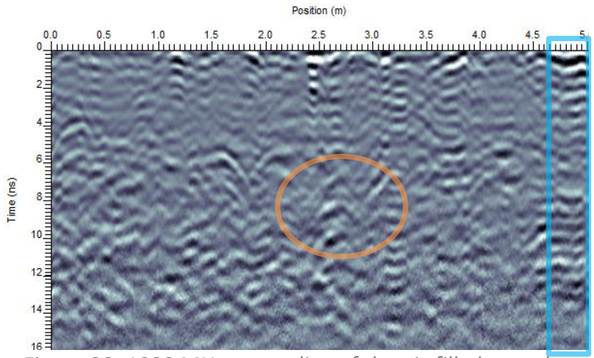

Figure 38: 1000 MHz survey line of the air-filled tunnel, no clear hyperbolic reflection. Highlighted in blue a vertical band of noise as result of poor ground contact.

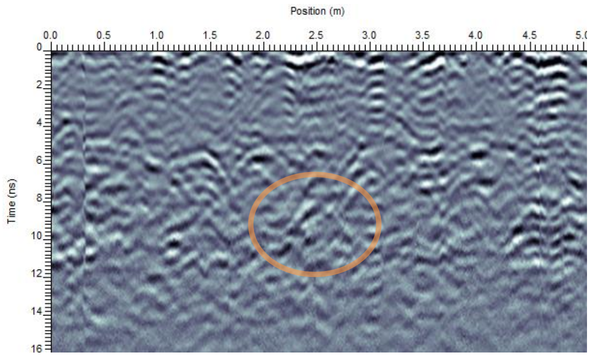

Figure 39: Almost identical to Figure 38 despite a metal pipe placed in the tunnel

8.1.4 Provisional conclusion

It can be concluded from the radargrams that the 250 and 500 MHz antennas are well capable in detecting the tunnel containing a metallic pole, giving a strong white-black-white reflection. When it is only air-filled, as is the case with a muskrat tunnel, the hyperbole is a black-white-black reflection and is significantly less strong which makes it difficult to distinguish from the surrounding reflections. However as the nesting rooms are usually bigger than 15 cm and the homogeneity of the surrounding soil may also vary, this is not yet a general conclusion. Although the 1000 MHz antenna yields the highest resolution the image is dominated by other scattering effects that make straightforward interpretation difficult. Hence it can already be qualified as unsuitable for the objective of this research.

8.2 GPR and ERT in sand at the Oostvaardersdijk

The long and outstretched bank at the Oostvaardersdijk consisted of a subsurface suitable for the ground penetrating radar. Figure 40 displays the sandy soil found with the hand borehole on site, confirming the lithology in Appendix A. The burrowing was expected to be mostly in the steep part of the bank, but the local muskrat controller and levee superintendent indicated it is highly probable that the tunnels go up into the flat bank and possible even to the foot of the levee slope. Consequently different grids have been measured with the ground radar. Unfortunately the ERT survey has been positioned as such that it did not include a known muskrat entrance, however still some remarks can be made.

8.2.1 Focus on entrance at waterside

The most interesting grid was measured on the steep part of the bank centred on a known entrance. The muskrat controller had identified the entrance half way the small 5 by 2 m grid (red arrow in Figure 42).

Figure 41 displays the 500 MHz antenna radargram of the survey line closest to the water, which corresponds to the line at 0.0 m on the vertical axis in Figure 44. Various black-white-black reflections are visible with a somewhat hyperbolic shape at position 2.5, 3.5, 3.7, 4.0 and 5.0 meters. Although one leg of the reflection at 2.5 m is stronger in amplitude it is identified as a hyperbole caused by the known tunnel entrance. With an estimated velocity of 0.1 m/ns (in between wet and dry sand) the 10 ns converts to a depth of 0.4 m, which is in accordance with the height difference between the survey line and the water level measured with the GPS. The adjacent surveyed line of Figure 43 shows hyperboles at similar locations and it appears that they are coming from the same object. The horizontal depth slice at 0.5-0.55 m (Figure 44) shows that the strength in amplitude continues forming a tunnel like shape, which seem to

Figure 40: Soil sample drilled on the bank showing difference in the upper and lower sand.

separate in branches after 0.75 m. A shallower depth slice from 0.4-0.45 m (Figure 46) shows high amplitudes upslope and from the slice it seems that the tunnels continue parallel to the water. However this is not in accordance with the radargram of Figure 45, surveyed upslope at 1.75 m. The high amplitude seems to come from more horizontal and continuous reflections hinting towards a subsurface layer. The horizons are interrupted by hyperbolic structures but they are less distinct than in the previous discussed radargrams, causing a more scattered image. Hence it is difficult to estimate the scope of the tunnel network by either the radargram or the horizontal slice or using a combination.

A different point of view is acquired by the three-dimensional visualization of the grid using Voxler. The data displayed in Figure 26 of Chapter 7 is filtered according to a certain isovalue, after which only the desired amplitude strength is preserved while all values lower and higher are left out. This resulted in Figure 47 showing the top and two side views of the grid. A tunnel-like shape can be identified starting halfway the waterside and separating in two branches, which appear to end further on. The tunnel network has differences in diameter; the wider part could be an indication of the presence of a nesting room. The reflections upslope do not appear to be part of the tunnel but seem more singular objects. A hand drilling nearby had been ceased as after 20 cm the hand drill found a rocklike object that the drill had not been able to penetrate through. At the waterside another tunnel shape is identified at 4 m position but shallower in depth (highlighted in purple in Figure 47). This could be an extra tunnel the muskrat digs in case it needs to disappear quickly but does not want to reveal the entrance of its burrow (Zuiderzeeland pers.comm.).

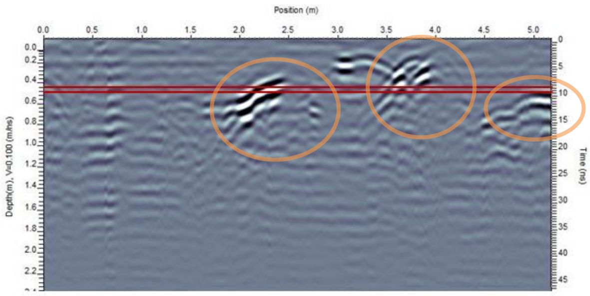

Figure 41: Survey at 0.0m of grid, red lines indicated depth slice at 0.5-0.55m. Positive peaked hyperbolic reflections visible also at 2.5 m position.

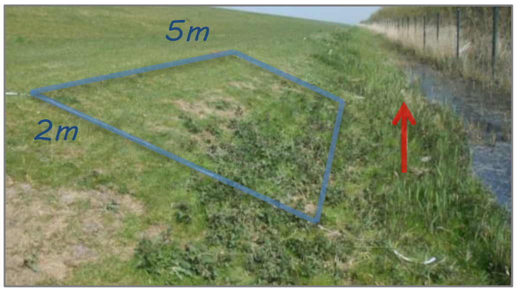

Figure 42: Grid 4 at Oostvaardersdijk with an entrance (red) at waterside halfway the grid.

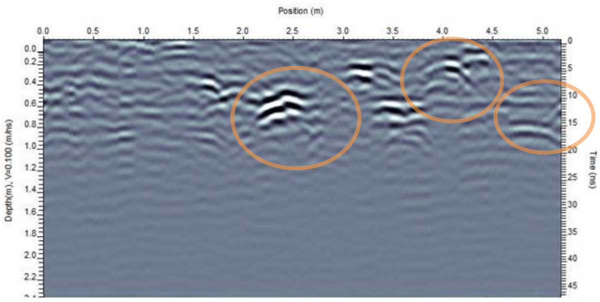

Figure 43: Line at 0.25m, hyperbolic reflections at similar positions as in Figure 44, they appear to continue

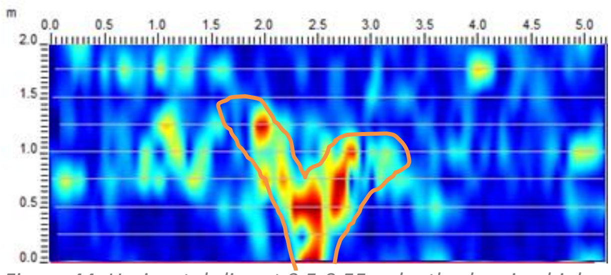

Figure 44: Horizontal slice at 0.5-0.55m depth, showing high amplitudes at position of a known entrance.

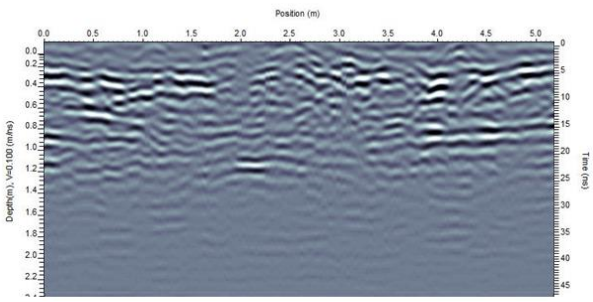

Figure 45: Line at 1.75m containing more reflections of which horizontal horizons and hyperbolic ones are less distinct.

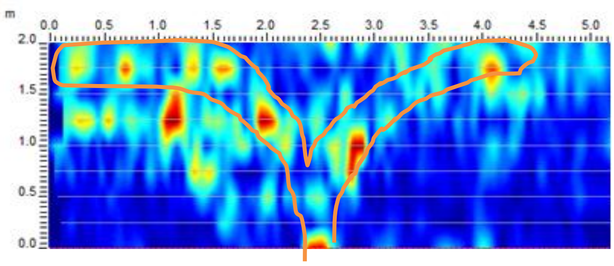

Figure 46: Slice at 0.4-0.45m depth, strong amplitudes are more scattered and less continues.

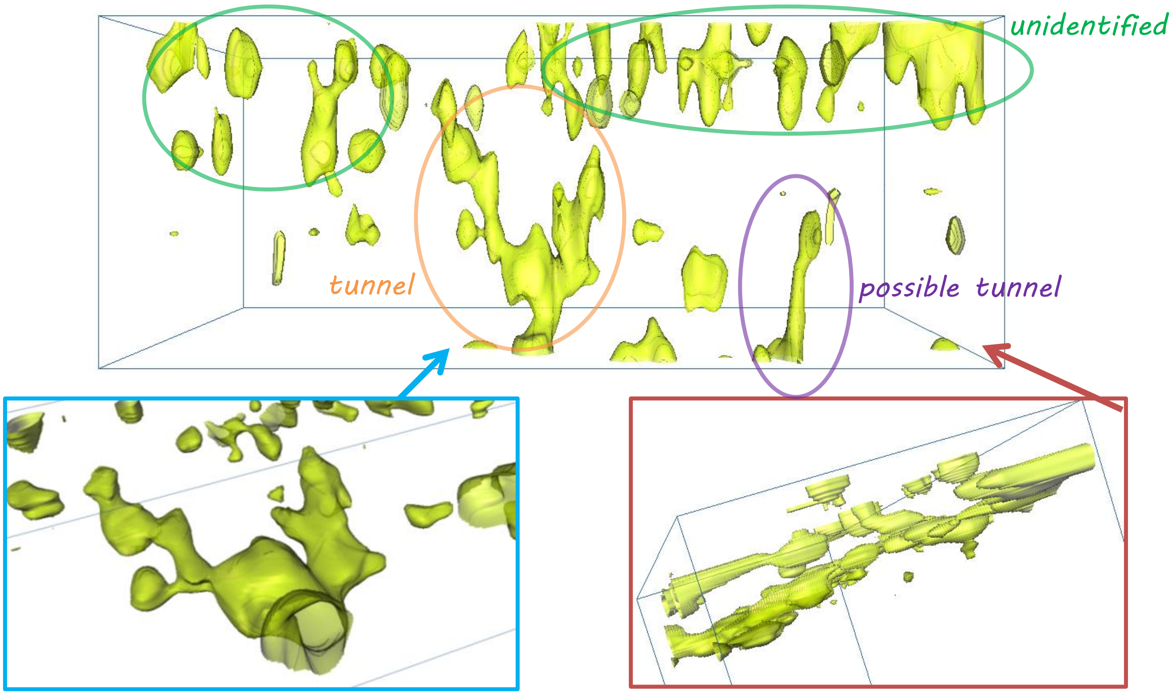

Figure 47: 3D visualization of Grid 4 in Voxler with top view (upper image) and two side views (bottom images) showing a tunnel shaped structure starting at the half way the grid at the water side continuing upward the steep bank.

Uncertainty estimation

The three-dimensional image used for interpretation depends on the assigned isovalue. Changing this value has quite an effect on the resulting image and must be handled with caution. Figure 48 displays the 3D grid when a lower (left) and a higher (right) isovalue is chosen. It is seen from the horizontal slices in Figure 44 and Figure 46 that the amplitude strength caused by an object smoothly decreases as the distance increases, from red to yellow to light blue. Even the light blue does not form a continuous and distinct body on the slices, which will also be the case for the 3D view. Choosing a lower isovalue results in a higher volume and the identified tunnel becomes thicker and even connected to the upslope objects that previously appeared to be singular. The unidentified reflections in the upper right corner imply now more a layer. Choosing a higher isovalue gives a much smaller volume and the tunnel become less identifiable as the left branch even disappears. It can be concluded that the isovalue must be chosen with care and in consideration with the radargrams and horizontal slices.

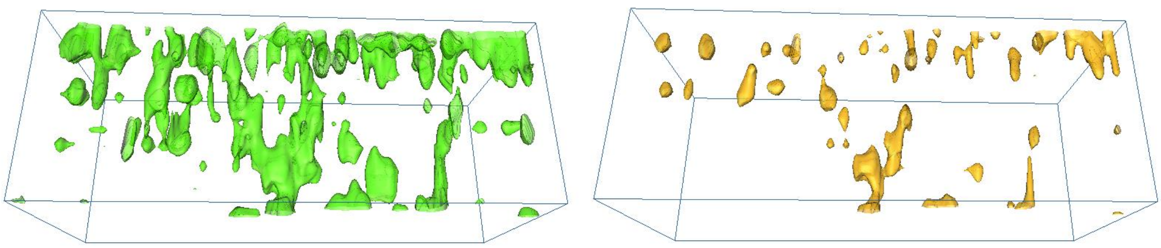

Figure 48: 3D visualization with left a lower isovalue showing more objects that cannot be related to a tunnel and right a higher isovalue gives a small volume.

8.2.2 The flat part of the bank

The grid on the flat part of the bank (Grid 3, Chapter 6 Figure 12) has been measured to investigate how far the burrowing goes up into the embankment. At position 3.3 m of the 3 by 12 meter grid an entrance is present down at the waterside. Figure 49 displays the radargram of the 500 MHz survey line at 2.75m on the vertical axis of the grid in Figure 50, which is located on the edge of the flat to steep bank. Distinct hyperbolic reflections are found around 7.5, 8 and 9.5 meters, which are at the position where the ditch did not contain water. As these hyperboles were visible on the console in the field it was attempted to discover its cause by a hand drilling. One borehole is displayed in Figure 40 showing surprisingly only wet sand followed by dry sand. As the velocity of wet sand is 0.06 m/ns (Table 2) this will be used for depth conversion. Two continuous horizontal reflections are dominant on all survey lines; the first is strong black-white-black, while the second is weaker white-black-white. The first horizons indicates $\varepsilon_1 > \varepsilon_2$, which is in coherence with the borehole and the relative permittivity of wet sand (10-30) and dry sand (2-6). The second horizon could be the water level, as $\varepsilon_1 < \varepsilon_2$ and it is also more horizontal that the first.

The intersecting hyperboles are difficult to analyse, on the radargrams they stand out from the horizons but on the slice in Figure 50 the hyperbole is not distinguishable. The amplitudes are of similar strength and merges together on the slice. Likewise are the two legs of the hyperbole at 8.25m position. On the radargram they are clearly visible, however this is not the case on the depth slices of Figure 51 (corresponding to the red lines in Figure 49). In Figure 51 the upper section is obtain with a normal gain and as this barely gave a signal the lower section has a more extreme gain applied. Nevertheless both fail to show a characteristic response that can be used to identify an anomaly. The 3D image of Figure 52 also only shows the structure of a layer and is not suitable for anomaly identification.

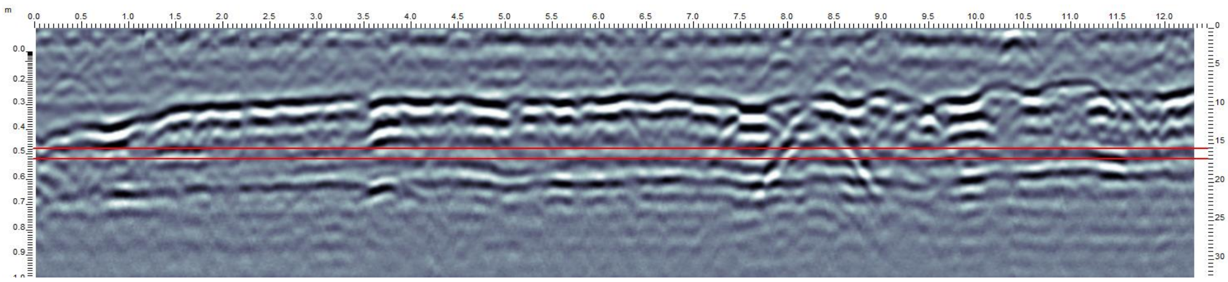

Figure 49: 500 MHz radargram of line at 3.75 m position on vertical axis of Figure 50. For depth estimation a velocity of 0.06 m/ns was used as sand was found to be saturated.

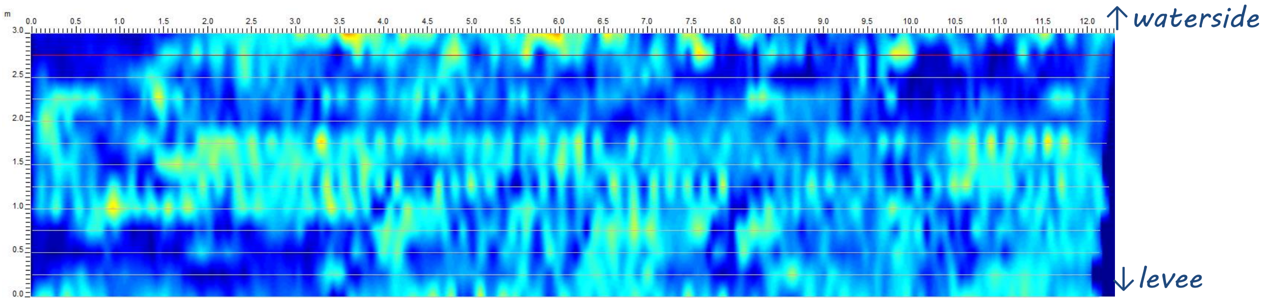

Figure 50: Horizontal slice at depth 0.30-0.35 m showing a more continuous reflection. The steep part of the bank begins at 3.0m on the vertical axis of this grid and

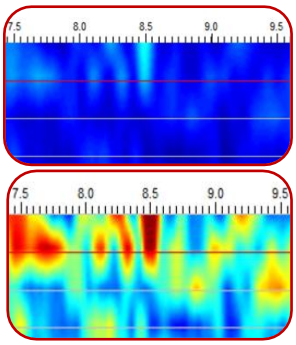

Figure 51: Slice focused on hyperbole legs at depth 0.48-0.52 m (red lines Figure 49) with normal gain (upper) and extreme gain (lower) applied

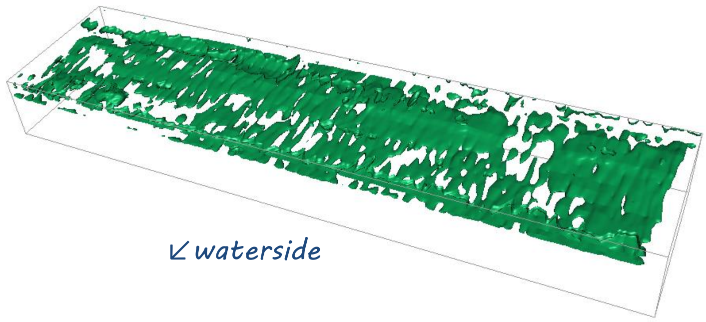

Figure 52: Horizon is 3D visualized, it is impossible to identify hyperbolic reflections

8.2.3 Detection when surveying large area

Previously the GPR results have been discussed of two grids that are relatively small, now the large grids will be discussed which have been surveyed on the steep (Grid 1) and the flat part (Grid 2) of the bank. The aim of the surveys was to investigate the ability of tunnel detection on a larger scale.

Steep part of the bank

Known entrances to the muskrat tunnels have been identified by the muskrat controller at 5.25 and 35.5 meters position of the grid. The line surveyed closest to the water is displayed in Figure 53, hyperbolic reflections are visible along with a horizon that changes in depth. Around the first entrance many hyperbolic reflections are present and some occur also at the same position on the adjacent survey line of Figure 54, however it is difficult to interpret that the anomalies are coming from a tunnel. This is also seen on the horizontal slices and the first 12 meters of the 3D visualization in Figure 55, which contain unreliable singular and more continuous structures.

Around the second entrance barely any reflection are visible. Moreover hyperbolic reflections that are present seem not to be continues on the adjacent survey line and do not indicate the presence of tunnels. Despite the identified entrance at the waterside, this part of the steep bank seems not to contain a burrow.

Between 15 and 28 m position on the line, the horizon is less distinct and the image contains clear hyperbolic reflections also present at similar depth and position on the adjacent survey line (Figure 54). However the 3D view of Figure 56 is again not helpful for tunnel identification. Unfortunately the console of the GPR failed to show these reflections in the field but this area would be of interest to investigate more thoroughly in the field by drilling holes.

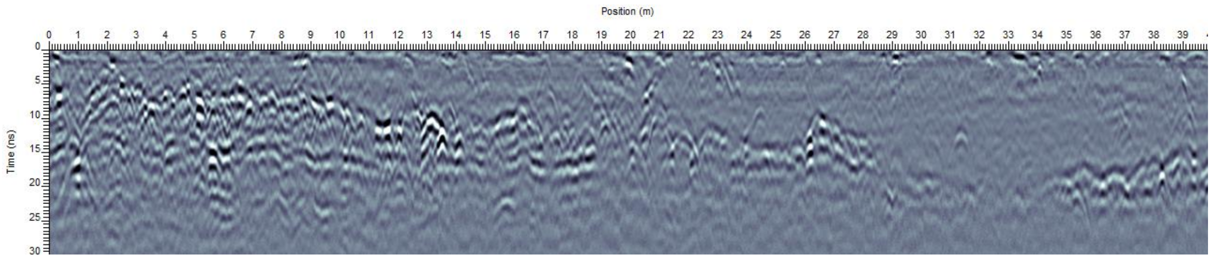

Figure 53: 500 MHz survey line 5, one meter down the steep bank. Hyperbolic reflections are visible.

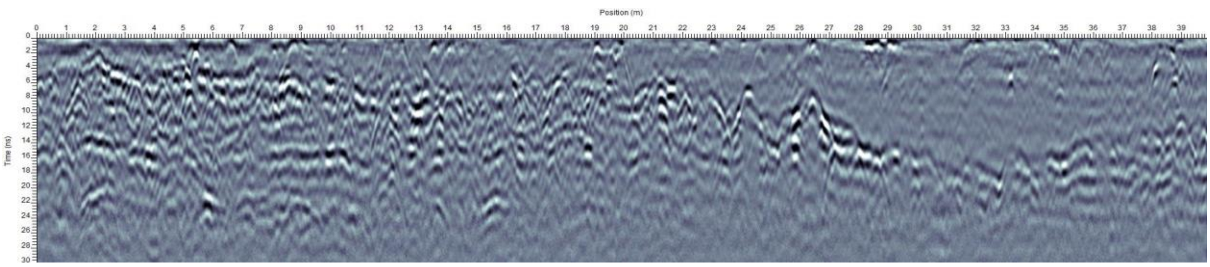

Figure 54: Adjacent survey line of, 0.75 meter down the steep bank.

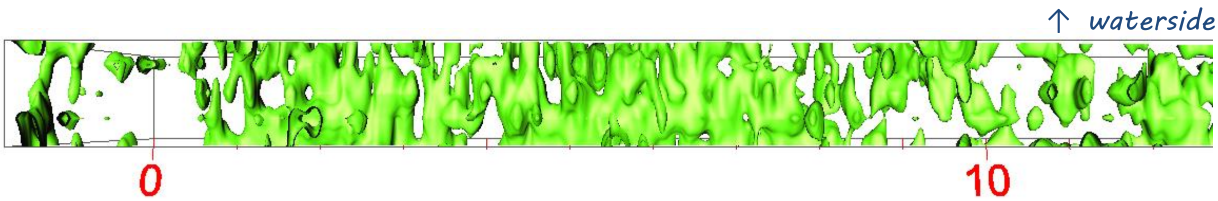

Figure 55: 3D visualization with of the first 12 meters of the grid containing the area of a known tunnel entrance.

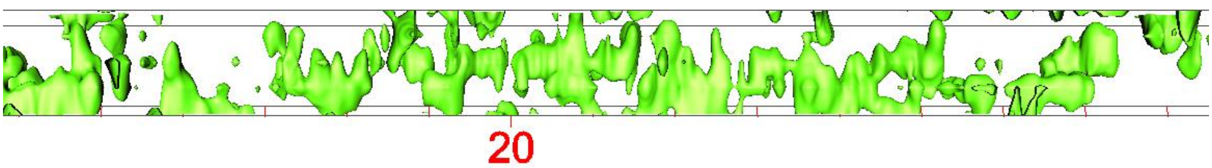

Figure 56: 3D visualization of the grid between 15 and 28 meters.

Flat part of the bank

In contrast to what was expected from the fieldwork, the results of the survey on the flat part of the bank did not provide evidence of animal cavities. The radargrams of the measured lines of Grid 2 all show the same continuous horizon of black-white-black origin. On site, three boreholes were made at assumed hyperbolic reflections visible on the console of the GPR. However on the computer it is seen that unfortunately these hyperboles are part of the horizon and not as result of an anomaly (Figure 57). The data contains numerous singular hyperboles but these are of lower amplitude strength and were not displayed on the console. Nevertheless they are not identified as part of a tunnel network as they are not continuous after more than one adjacent survey line and more possible the result of singular objects.

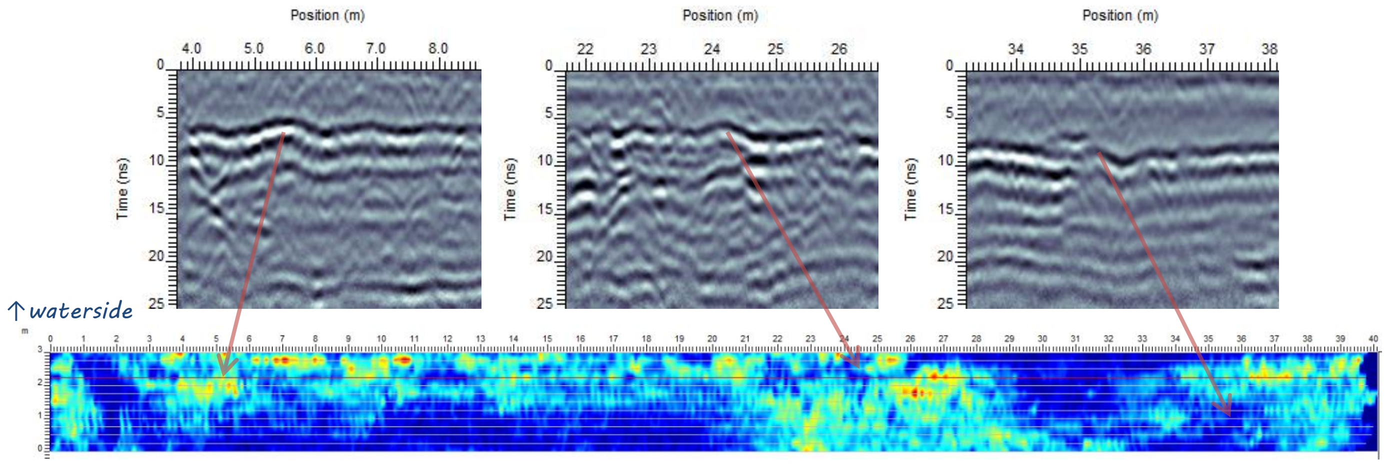

Figure 57: Three borehole drilled at 5.6 m (left), 24.5 m (middle) and 35.7 m (right) position at various survey lines on the grid (horizontal slice at 0.4-0.45 m/ 5-10 ns depth).Holes reveal that the hyperbolic reflection on the console of the GPR in the field belong to the continues horizon.

8.2.4 Interpreting ERT sections

As noted, due to the high vegetation on the day of the measurement the resistivity survey has been wrongly positioned. The near 21 meter survey was to include Entrance 1 (denoted in Figure 13 of Chapter 6) and its surroundings, but now merely reaches Entrance 2. Additionally the survey was slightly more downslope than the GPR survey of Grid 1, thus no real overlap was obtained. Nevertheless a comparison is made between the GPR survey in Figure 58 and the ERT section of Figure 59 and 60. The resistivity section of the Dipole-Dipole survey better resolves features in the near-surface than the Wenner. The Wenner section shows only higher resistivity areas around 2, 4, 6 and 11 m position at a depth of 0.4 m, whereas the Dipole-Dipole gives much more information.

The Dipole-Dipole sections show a background of lower value resistivity (around 35 Ωm) with areas of higher values up to 300 Ωm and lower values after a depth of 2.2 m (around 5 Ωm). A rough interpretation of the section is a sandy subsurface containing high-resistivity anomalies and at 2 m depth a saturated zone. Analysing with exclusively the resistivity sections the small high-resistivity areas in the near surface are assumed to be air-filled cavities.

High-resistivity areas on the Dipole-Dipole section occur and similar position and depth as reflections of interest on the GPR radargram. Highlighted in red in Figure 58 are reflections of black-white-black origin which are interpreted as possible air-filled tunnels. However further investigation in the field is necessary for confirming these assumptions. The reflections at 18 and 26 meter position on the radargram are white-black-white as is not interpret as an air-filled tunnel. At 31 m the crest of a hyperbole is visible corresponding to a high resistivity area, however on the adjacent GPR survey lines this reflection is not continues and thus it is not interpret as a tunnel.

Analysing the resistivity sections has not provided a conclusive identification of the muskrat tunnels. Moreover it is only a 2D section and does not provide spatial information that is highly desired for the objective of this research.

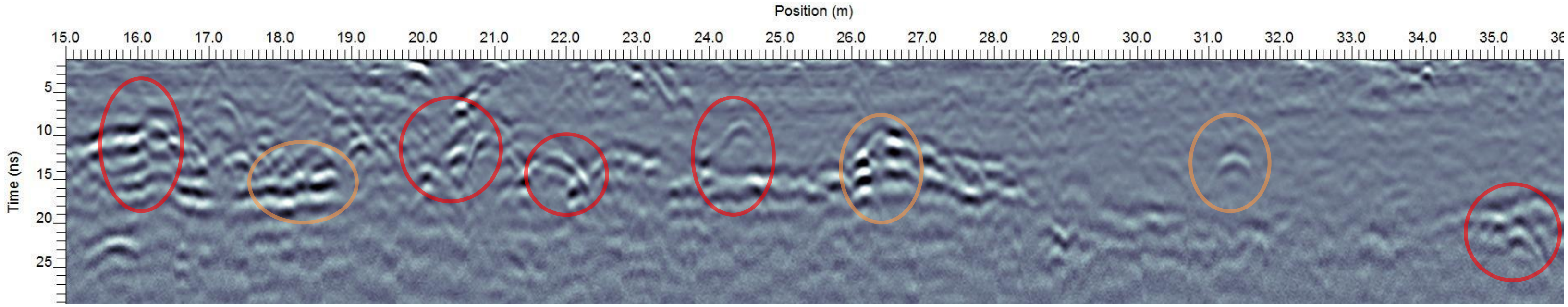

Figure 58: The near overlapping part of the GPR survey line 4 of grid 1 measured with the 500 MHz antenna corresponding to Figure 53. Highlighted in red are reflections that are identified as air-filled tunnels after comparison with the Dipole-Dipole resistivity section. The orange highlighted reflections remain unidentified.

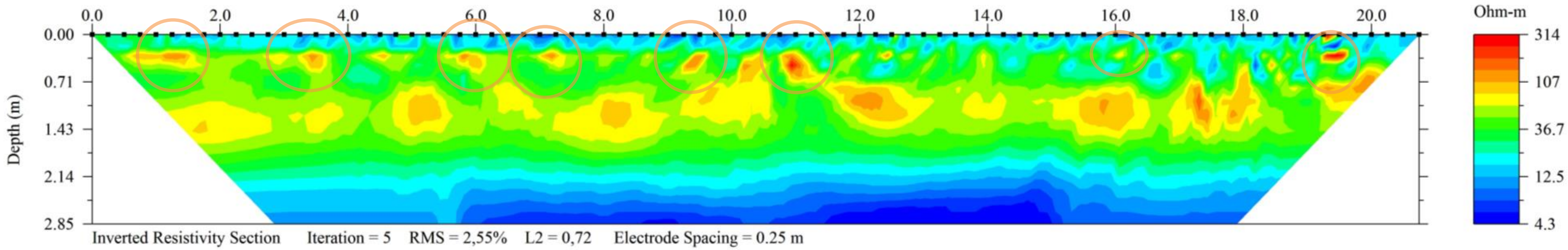

Figure 59: Dipole-Dipole resistivity section with highlighted in orange interesting anomalies of high resistivity. These are interpret as air-filled cavities and are further compared to the GPR radargram of Figure 58.

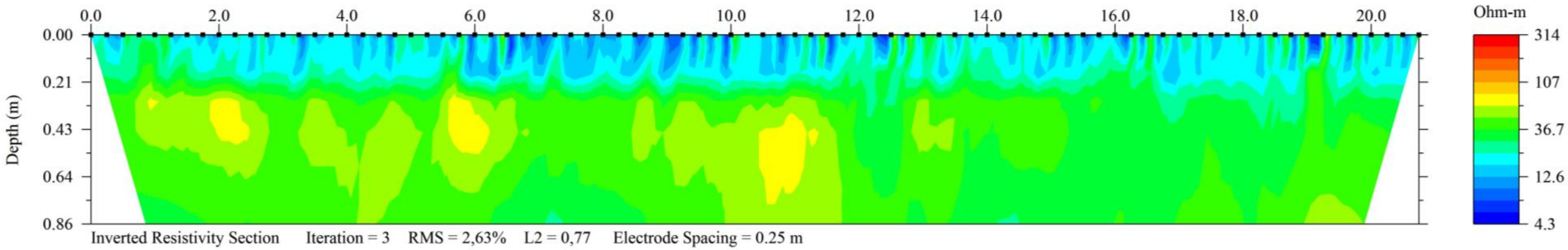

Figure 60: Resistivity section of the Wenner survey. Colour scale is set to correspond to the scale of the Dipole-Dipole section for better comparison. Default scale of the Wenner sections is display in Appendix D.

8.3 Peat and clay at the Alblasserwaard

Prior to the fieldwork it was expected that the area was suitable to investigate the detection of small cavities in a subsurface of peat. It proved however that the peat was generally covered with clay, which was in accordance with afterwards found borehole information from the DINOloket database. At the first location a top layer of clay with a thickness of around 50 cm (Figure 61) was confirmed with the hand drill (Figure 62). A layer of 15 cm was measured at location 2 (Figure 63) and 30 cm at location 3 (Figure 64). These top layers are usually too thick for the ground radar to sufficiently receive signals from subsurface reflectors. Nevertheless at the location 1 and 3 some interesting results are worth discussing and at location 2 it was even possible to measure a grid.

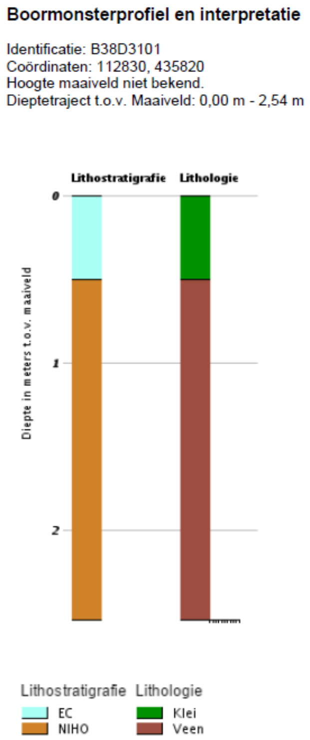

Figure 61: Drill sample profile indicating a lithology (right column) of a 50 cm thick clay layer (green) above peat (brown). (DINOloket 2015)

Figure 62: Borehole at location 1 with a 50 cm clay layer present above the peat (black)

Figure 63: Borehole at location 2, with 15 cm clay layer

Figure 64: Borehole at location 3 near the waterside with assumed tunnels. A 30 cm top clay layer was found.

8.3.1 Location 1

In contrast to the 50 cm clay layer found at the waterside another drilling in the centre of the field showed only of peat. The clay could possibly be applied as top layer against subsidence of concrete road constructed close to the water. The survey line showed that the clay layer was not as thick and impenetrable everywhere. The best radargram has been obtained with the 500 MHz antenna (Figure 65), as poor resolution resulted with the 250 MHz and 1000 MHz.

Three holes were drilled at reflections visible on the GPR console occurring at 4.5, 5.3, and 10.9 m position, the first two found actual tunnels. Figure 65 also shows the borehole at 4.5 m with the little amount of ground brought up to the surface, not containing clay. The velocity of the hyperbolic reflection at 4.5 m is estimated as 0.067 m/ns, this is in accordance with the literature values in Table 2. Figure 62 displays the drilling at 10.9 m with the thick clay layer but fails to visualize the ground water level, which has been found at 1.1 m. However on the radargram the level is visible as a horizontal white-black-white reflection at 20 ns which converts to 0.75 m with Equation 5. The difference in depth could be explained by the inaccuracy of the hand drill as small amount of soil are laid on the surface, where loose soil gets spread out and expand in length. Moreover loose soil like peat can collapse from the side of the hole, giving a greater volume.

The muskrat controller had indicated entrances at the waterside on positions 0.8, **2.0**, 2.8, **3.6**, 4.2, **4.6**, **5.3**, 5.9, 7.5, **8.3,** 9.0, 12.0, **12.7** and 13.4 meters. Highlighted in bold are positions that show a hyperbolic reflection on the radargram (highlighted in green Figure 65). Although the reflections are not distinct it is interpret that these are coming from the tunnels as reflections are black-white-black. The remaining entrances are possibly not visible on the radargram due to a local presence of clay. The unedited radargram of is found in Appendix D.

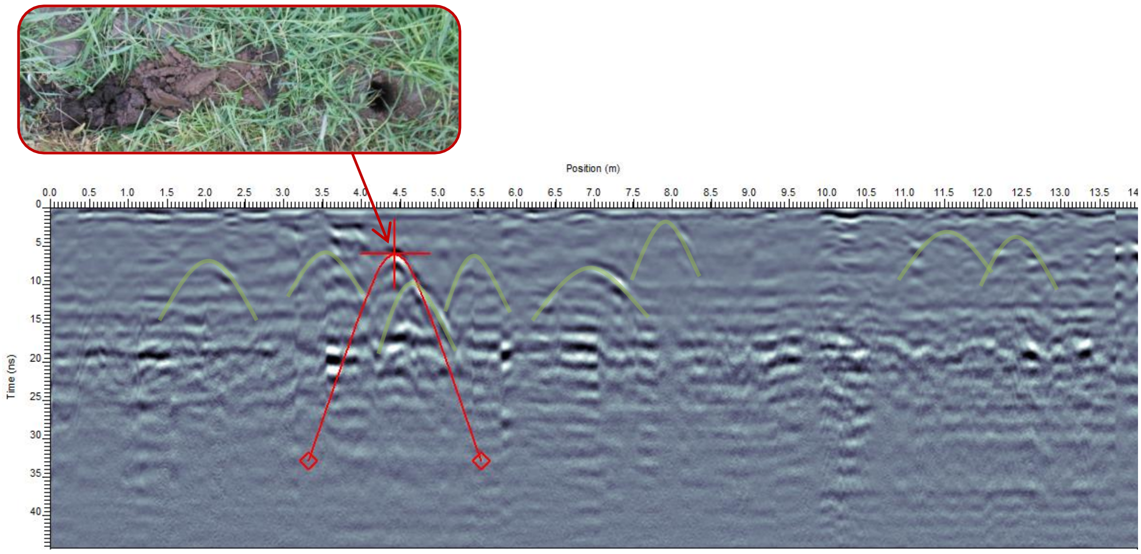

Figure 65: Radargram of 500 MHz antenna survey line at Location 1. Borehole at 4.5 meters discovered an air filled cavity, also indicated by the hyperbolic reflector (red). The velocity is estimated as 0.067 m/ns. Other hyperbolic reflections in green are possible animal tunnels as flags have indicated entrances at the water side.

8.3.2 Location 2

Despite the clay layer found with the drill reflections have been received from the subsurface, especially on the first survey line directly at the water side (Figure 66). At 2.2 meters along this line a 20 cm wide tunnel has been identified by the local muskrat controller. A horizontal depth slice at 0.15 till 0.20 m is shown in Figure 67, in which interpretations are included. Depicted in orange is the tunnel network estimated by the controller, who used his metal pricking tool to poke the ground. The tunnel started at the waterside and went around the tree at position 2.8 m, whose roots are a preferred place for muskrats to create their tunnel as the soil is more loosened. High reflections are visible at the expected position in the colours green, yellow and red, however they are also present on the left of the grid. This was not clearly seen in the field on the console of the GPR, and as such remains unidentified. Another depth slice ranging from 0.6-0.65 meters (Figure 68) indicates similar high amplitudes around 2.0 and 3.8 meters, which could also be interpreted as the entrances at the waterside, since the embankment is about that high. Overall the horizontal slices are not full-prove, and without knowing the presence of a burrow it is not interpreted as such.

Looking at the three-dimensional image of Figure 69, it is seen that most of the strong amplitudes are at the waterside. It appears that at 2.8 m position a long round shaped reflection is from the trunk of the tree. At greater depth around and at 2 m position the supposed tunnel does form a similar shape. The unidentified high amplitudes on the left of the grid can still not be defined as an entrance for certain. The three different perspectives of the data show that it is difficult to identify the tunnel from surrounding reflections.

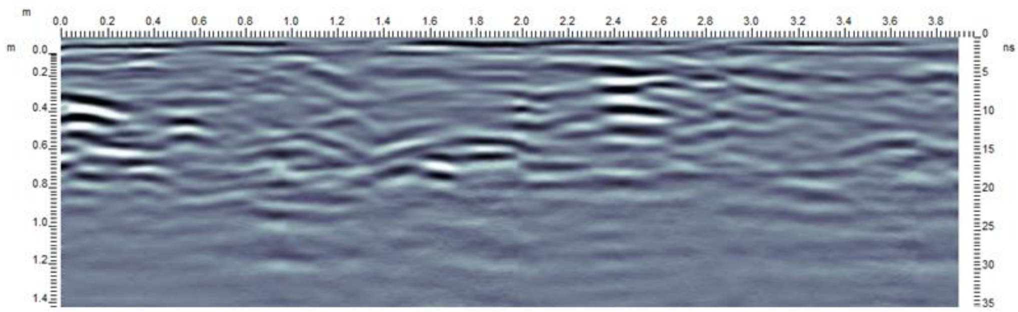

Figure 66: Location 2 500 MHz survey line at position 0 m of the grid, located next to the water with a tree at 2.8 m and a tunnel at 2.2 m. Various reflections from the subsurface are visible.

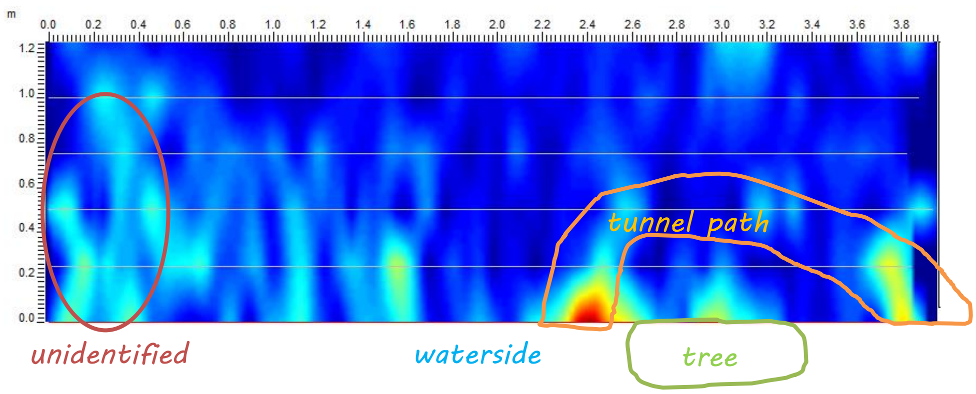

Figure 67: Depth slice at 0.15-0.20 m, grey lines indicate the surveyed line with 0.25 m interval. Line 0.0 m on the vertical axis is the radargram of Figure 66. Highlighted in orange is the muskrat controller's estimation of the tunnel network. At 2.8 m a tree is present and an unidentified signal at 0-0.4 m.

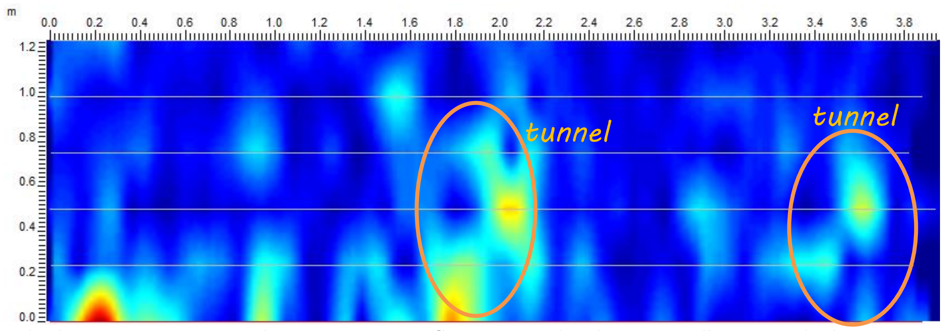

Figure 68: Depth slice at 0.60-0.65 m showing strong reflection amplitude at 1.8 till 2.2 m which is interpret as possibly coming from a muskrat tunnel

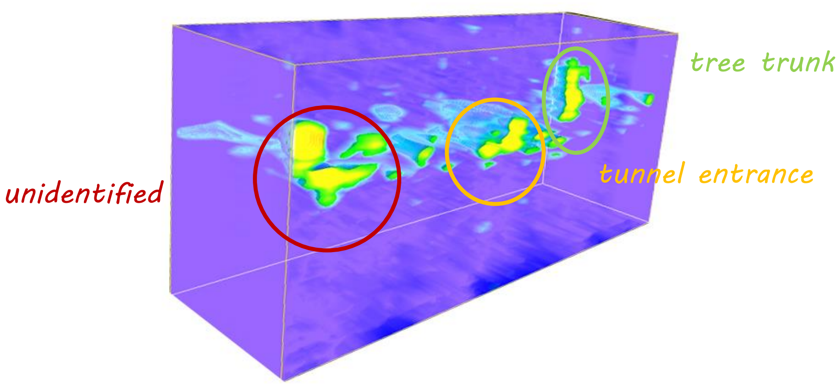

Figure 69: 3D image of the gird shows strong reflections mostly on the waterside and between 0.15 and 0.6 meters deep. The trunk of the tree is identifiable, but the shape of the tunnel is less clear. In the field the GPR failed to show the later unidentified reflections denoted in red.

8.3.3 Location 3

The test survey line near the waterside resulted in a radargram with no reflections from the underground (Figure 70). The hand drill then indicated that the clay layer was too thick for the signal to penetrate through (30 cm as shown in Figure 64). More lines were surveyed on the meadow out of curiosity whether the clay layer was as thick everywhere. One line gave halfway surprisingly many reflections (Figure 71). At a reflection visible on the console of the GPR, 6 meters along the line, a hole was drilled to attempt to obtain the causing reflector. This drilling brought a lot of plastic threads and fine shredded wood to the surface. As near all reflections show a negative peak, it is assumed also from the debris that came to the surface that part of the meadow ground was filled construction waste. A drain cut through the field at around 10 meters and contained water which is visible in the radargram as a strong white-black-white reflection.

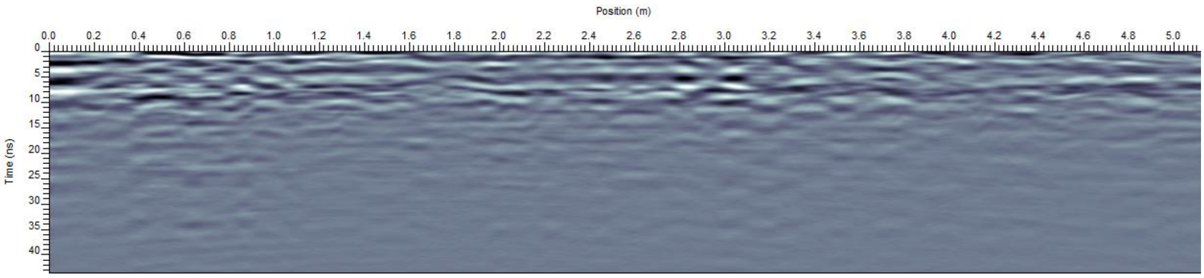

Figure 70: Radargram of 5 m survey line near waterside at location 3, measured with the 500 MHz antenna. No reflections are present due to the thick layer of clay as was discovered by the hand drill.

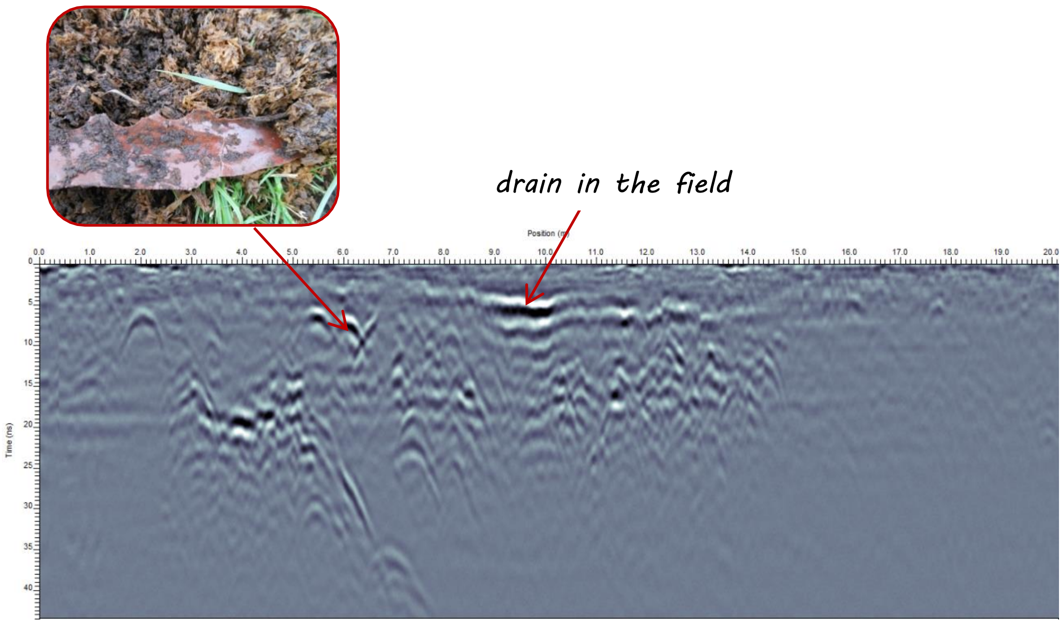

Figure 71: Radargram of 20 m survey line across the meadow at location 3, measured with 500 MHz antenna. Reflections occur between 2.5 and 14.5 meters along the line, possibly due to construction debris filling. After 14.5 meters no reflections from depth due to the top clay layer. Borehole at 6 meter reflection found plastic and shredded wood.

8.4 Discussion

During the fieldwork some setbacks have been accounted that considerably slowed down the data acquisition and its analysis. Survey parameters had been wrongly assigned and surveying had to be redone. Nevertheless the instruments had also some limitations themselves, of which mainly the console of the pulseEKKO PRO. The radargram on the console is of poor resolution and failed to show anomalies of interest, which had later been visible on the computer software. Consequently, most anomalies remain unidentified and assumptions made in this report have not been ground truth by use of the hand drill. Nevertheless some boreholes confirmed a subsurface air-filled cavity while others identified layered structures and random objects. In retrospect it is preferred to analyse the data with the software directly in the field, in order to investigate the interesting anomalies.

The dominant presence of clay at survey sites had not been expected and gave problems to the penetration of the radar signal. Finding a suitable sandy subsurface has been difficult as most embankments are sealed with a clay layer against erosion. Furthermore the physical structure of the embankments are often not as desired, either too steep, tortuous or rough for proper GPR surveying. High vegetation encountered on the field days during May till June gave problems for the accessibility and the ground coupling of the instrument. The muskrat management organisations desire a method or instrument which is applicable to a significant majority of embankments all year long, thus these limitations of the GPR must be taken in serious consideration.

Analysing the acquired GPR data showed that the 500 MHz antenna gives sufficient resolution for the desired depth of investigation. Lateral changes are well detected and two close objects at the same depth are shown as two separate anomalies. The results of the 1000 MHz antenna show too much scattering in which desired reflections are hard to see by straightforward interpretation. Hence it is not the most informative data set for this objective. The 250 MHz managed to image similar reflections as the 500 MHz but the discrimination of single tunnels decreased with increasing depth. Additionally, the deeper part of the 250 MHz radargram has not been of interest as tunnels have not been identified to be present here.

Performed near the end of the research, the test tunnel in the Wapenveld area gave a most interesting result. The air-filled tunnel appeared as a hyperbolic reflection at expected position and depth on the radargram. The reflection, less strong than when the hole contained a metal pole, showed a black-white-black reflection or a positive peak as response of a transition from a larger to smaller relative permittivity. In contrast a smaller to larger relative permittivity will result in a negative peak and a white-black-white reflection on the radargram. This can occur when a cavity is filled with water or a sand anomaly is surrounded by clay. The reflection coefficient is not unique for a typical boundary, however its polarity can assist in the interpretation of anomalies. In retrospect additional test measurements would have been preferred to better understand the GPR signal. The test tunnel was now placed at 20 cm depth and went straight into the slope, it would have been interesting to investigate a deeper and wider tunnel that curved in the subsurface. However the steep site is not safe to create such a test setup.

Analysing the radargrams and horizontal slices for the presence of muskrat tunnels proved to be more difficult than expected. In the case of a sandy and homogeneous soil the hyperbolic reflections are quite distinct and identification is relative easy. In a heterogeneous sandy soil as at the test tunnel of the Wapenveld area the hyperbolic reflections is difficult to identify if its presence had been unknown. In a layered subsurface as the flat part of the bank at the Oostvaardersdijk the hyperboles are detectable on the radargrams but their amplitude strength merges with the horizons having similar strength, and become undetectable on the horizontal slices. This problem is similar with the 3D visualization in Voxler, as the isovalue is filter for one specific amplitude strength. In case of the small Grid 4 centred on the tunnel entrance the 3D view has been able to give advanced insight on the tunnel network, but with others grids it failed in doing so. Another drawback in Voxler is the data file size when the grid dimensions are large. When the desired 3D resolution of 2 cm by 2 cm is chosen the files becomes too large to work with. This is not practical as for application by the muskrat organisations in mind it is desired to survey kilometres of embankments in one go.

With the processing of the GPR signal many advanced options are available and are in general similar to those of seismic data processing. However the effects on resolution of the GPR data are not that interesting. To resolve the problem with the legs of the hyperbole reflection migration can be applied to convert the hyperbole to a single point at its origin. However this was not attempted in this research.

The electrical resistivity survey has been positioned as such that it did not completely overlap a GPR survey or include a tunnel entrance. However the measurement did give insight in the application of the method to the muskrat problem. Being time-consuming in both the measurement and setup which is also labour-intensive the method results in a too poor resolution of the subsurface. Additionally, only one survey line can be measured per setup, thus no information on the spatial extent is obtained. This is disadvantageous as it remains unknown if the anomalies that are found are continuous on adjacent sides.

Chapter 9

Conclusions

At present muskrat management organisation are responsible for managing the muskrat population. They do that by visually inspecting embankments and utilizing both lethal and non-lethal catching methods. With this research a study has been performed to approach the problem by using geophysical methods. As outcome it has been found that most methods do not provide a sufficient resolution to distinguish the tunnels from the surrounding soil and their disadvantages are too great for realistic and practical application. On various embankments in three areas in the Netherlands measurements have been performed with the ground penetrating radar and electrical resistivity tomography to evaluate their ability to detect small animal cavities in the near surface. In addition, the methods have been analysed on their capability to visualize the spatial extent and depth of the tunnel network in a sandy, clay and peat subsurface.

Fieldwork with ground penetrating radar showed in all areas that the best resolution in the desired depth of investigation is obtained with the 500 MHz antenna. An artificial tunnel created in a sandy embankment at 20 cm depth has successfully been detected. In the presence of the tunnel a hyperbolic reflection appeared causing a positive peak in the trace signal, or a black-white-black reflection on the radargram. This property can be used to discriminate an air-filled tunnel from for example a water-filled cavity or a rock, which shows a white-black-white reflection.

GPR has successfully been applied at the Oostvaardersdijk which consisted of a sandy soil. Here a survey centred on a known tunnel entrance gave reflections at expected positions and continued on adjacent survey lines. Additional insight on the scope of the tunnel network has been obtained with the horizontal slices and the 3D visualization. However, with a layered subsurface the intersecting hyperbolic reflections are poorly visible on the slices and only the radargrams can be used. A spatial visualization of the cavities has not been achieved in most of the measured grids. Surveying a large area, as will be the case in practice, gave countless anomalies whose interpretation is time-consuming and full of uncertainties.

A thick layer of clay prohibits the GPR signal to penetrate through the subsurface. A majority of embankments in the Netherlands have a top clay layer against erosion. Additionally, many embankments are unsuitable for realistic surveying due to their structure or seasonal vegetation.

The Dipole-Dipole survey gave a more detailed and reliable resistivity section than the Wenner survey. However the cross-section that was difficult to interpret without additional information from GPR surveying. Additionally the measurement includes only one survey line which is labour-intensive in its setup and time-consuming in it measurement. Moreover it does not provide information on the scope and spatial connectivity of the network.

To conclude, ground penetrating radar is the best suited method for detecting the burrows of the muskrat, however it is not realistic for application by the management organisations. The anomalies of interest are not sufficiently distinguished from other anomalies and subsurface structures. The visualization of the spatial extent and connectivity of the tunnel network is not reliable. Moreover the data acquisition and interpretation is too time-consuming and labour-intensive to replace or complement the current way of management.

References

Akkermans M. (2014) Invloed van graverij muskusratten op de waterveiligheid. Amersfoort, STOWA, report 451.211

Allred B.J., Groom D., Reza Eshani M., Daniels J.J. (2008) Handbook of Agricultural Geophysics Chapter 5 Resistivity methods. Taylor & Francis Group LLC

Baker G. S., Schmeissner C., Steeples D.W., Plumb R.G. (1999) Seismic reflections from depths of less than two meters. Geophysical Research Letters 26(2):279-282

Bayoumi A., Meguid M. A. (2011) Wildlife and Safety of Earthen Structures: A Review. Journal of Failure Analysis and Prevention 11(4):295-319

Beard L.P., Nyquist J.E., Carpenter P.J. (1994) Detection of karst structures using airborne EM and VLF. Presented at SEG Annual International Meeting, 1994

Benson A.K. (1995) Application of ground penetrating radar in assessing some geological hazards: examples of groundwater contamination, faults, cavities. Journal of Applied Geophysics 33:177-193

Biavati G., Ghirotti M., Mazzini E., Mori G., Todini E. (2008) The use of GPR for the detection of non-homogeneities in the Reno River embankments (North-Eastern Italy). 4th Canadian Conference on Geohazards, Université Laval, Québec, Canada, 20–24 May

Bos D., Tuenter T. (2007) Muskusratten zonder bestrijding? Ontwerp van een onderzoek aan de gevolgen van tijdelijk niet bestrijden. Altenburg & Wymenga, A&W-report 1032

Butler D.K. (1984) Microgravimetric and gravity gradient techniques for detection of subsurface cavities. Geophysics 49(7):1084–1096

Chlaib H.K., Mahdi H., Al-Shukri H., Su M.M., Catakli A., Abd N. (2014) Using ground penetrating radar in levee assessment to detect small scale animal burrows. Journal of Applied Geophysics 103:121-131

Daniels D.J. (2004) Ground Penetrating Radar 2nd Edition. The Institution of Electrical Engineers London ISBN: 0-86341-360-9

Daniels J.J., Vendl M., Reza Ehsani M., Allred B.J. (2008) Handbook of Agricultural Geophysics, Chapter 6 Electromagnetic Induction Methods. Taylor & Francis Group LLC

Di Prinzio M., Bittelli M., Castellarin A., Rossi Pisa P. (2010) Application of GPR to the monitoring of river embankments. Journal of Applied Geophysics 71:53-61

DINOloket (2015) Data en Informatie van de Nederlandse Ondergrond. https://www.dinoloket.nl/

EarthImager 2D Manual (2009) Instruction Manual of AGI EarthImager 2D. Resistivity and IP Inversion Software Version 2.4.0 Advance Geosciences, Inc. Austin

EKKO_Project Manual (2015) EKKO_Project User's Guide. Sensors & Software Inc. Canada

El-Qady G., Hafez M., Abdalla M.A., Ushijima K. (2005) Imaging subsurface cavities using geoelectric tomography and ground-penetrating radar. Journal of Cave and Karst Studies 67(3):174-181

Environmental Geophysics (2011) Basic Information on Geophysical Methods Basic Concepts. U.S. Environmental Protention Agency Offical Website

Everett M. E. (2013) Near-Surface Applied Geophysics. Cambridge University Press eISBN 9781107345355

Feldhamer G.A., Thompson B.C., Chapman J.A., (2003) Wild Mammals of North America: Biology, Management, and Conservation. The Johns Hopkins University Press ISBN: 0-8018-7416-5

Foti S., Lai C.G., Rix G.J. Strobbia C. (2014) Surface wave methods for near-surface site characterization. CRC Press ebook ISBN 9781482266825

Ghafarian Malamiri H.R. (2015) Reconstruction of gap-free time series satellite observations of land surface temperature to model spectral soil thermal admittance. Doctoral Dissertation, Technical University Delft

Goodman D., Piro S. (2013) GPR Remote sensing in Archaeology. Springer Geotechnologies and the Enviroment ISBN 078-3-642-31857-3

Hansje Brinker (2012) Hansje Brinker B.V. http://hansjebrinker.com/

Heidinga D. (2006) Pluizige plaagdieren. Onderzoek naar de ecologie van de muskus- en beverrat in Nederland vanuit een populatie dynamisch perspectief bekeken. Rijksuniversiteit Groningen, Wetenschapswinkel Biologie, report 70

Huenecke H.S., Erickson A.B., Marshall W.H. (1958) Marsh gases in muskrat houses in winter. The Journal of Wildlife Management 22(3):240-245

Johnson W.J., Snow R.E., Clark J.C. (2002) Surface geophysical methods for detection of underground mine workings. Conference: Symposium on Geotechnical Methods for Mine Mapping Verifications

Jol H. M. (2009) Ground Penetrating Radar Theory and Applications. Burlington Elsevier 2009, ISBN 9780008951843

Kang Y.V., Hsu H. (2013) Application of ground penetrating radar to locate shallow cavities in a coastal dyke. Journal of Applied Science and Engineering 16(1):23-28

Konstantaki L. A., Carpentier S., Garofalo F., Bergamo P., Socco L.V. (2013) Determining hydrological and soil mechanical parameters from multichannel surface-wave analysis across the Alpine Fault at Inchbonnie, New Zealand. Near Surface Geophysics 11:435-448

Konstantaki L. A., Ghose R., Draganov D., Heimovaara T. (2015) A geophysical toolbox for imaging and characterization of a landfill. HPM6: The 6th International Workshop Hydro-Physico-Mechanics of Landfills, Delft, 14-17 April 2015

Kovalenko V.O., Van Isselt C. (2014) Pilot GPR scan muskusrattenholen. Fugro Geoservices B.V. opdrachtnummer 1514

Lammertsma D.R., Niewold F.J.J. (2005) Muskusrattenbestrijding in Nederland: een quick scan naar nut, noodzaak en alternatieven. Wageningen, Alterra, Alterra-report 1197

Mochales T., Casas A.M., Pueyo E.L., Pueyo O., Román M.T., Pocoví A., Soriano M.A., Ansón D. (2008) Detection of underground cavities by combining gravity, magnetic and ground penetrating radar surveys: a case study from the Zaragoza area, NE Spain. Environ Geology 53:1067-1077

Munk J., Sheets R.A. (1997) Detection of underground voids in Ohio by use of geophysical methods. U.S. Geological Survey Water-Resources Investigations Report 97-4221

Muskrat management (personal communication) Information obtained from various organisations and persons of which Zuiderzeeland (Michael Baars, Klaas Post, Fokke Jonkman), Vallei en Veluwe (Lambertus van Diermen), Rivierenland (Anton Deelen), Schelestromen (Peter Blanker), Brabantse Delta (Pieter Verhoeven), Vechtstromen (J. Hekman)

PulseEKKO PRO Manual () PusleEKKO PRO User Manual Sensors & Software Inc. Canada

Putiska R., Nikolaj M., Dostal I., Kusnirak D. (2012) Determination of cavities using electrical resistivity tomography. Contribution to Geophysics and Geodesy 42(2):201-211

Revil A., Karaoulis M., Johnson T., Kemna A. (2012) Review: Some low-frequency electrical methods for subsurface characterization and monitoring in hydrogeology. Hydrogeology Journal 20:617-658

Saey T., Van Meirvenne M., De Pue J., Van De Vijver E., Delefortrie S. (2014) Reconstructing mole tunnels using frequency-domain ground penetrating radar. Applied Soil Ecology 80:77-83

Smith D.G., Jol H.M. (1995) Ground penetrating radar: antenna frequencies and maximum probable depths of penetration in Quaternary sediments. Journal of Applied Geophysics 33:93-100

Socco L.V., Strobbia C. (2004) Surface-wave method for near-surface characterization: a tutorial. Near Surface Geophysics 165-185

Stern W. (1929) Versuch einer elektrodynamischen Dickenmessung von Gletschereis: Beiträge zur Geophysik 23:292-333

Tzanis A. (2010) matGPR Release 2: A freeware MATLAB® package for the analysis & interpretation of common and single offset GPR data, FastTimes 15(1):17-43.

Union of Water Authorities (2014) Landelijk jaarverslag 2013 Muskus- en Beverratten. Den Haag Bijlage CMB 14-8b

Union of Water Authorities (2015) Landelijk jaarverslag 2014 Muskus- en Beverratten. Den Haag 1 juni 2015

Van Hemert H., Spoorenberg C. (2006) Gevolgen van graverij door muskusratten en beverratten voor de veiligheid van waterkeringen. DHV Groep BCM Amersfoort dossier A2998.01.001

Yang X., Henderson G., Mao L., Evans A. (2009) Application of ground penetrating radar in detecting the hazards and risks of termites and ants in soil levees. Environmental Entomology 38(4):1241-1249

Appendix

Appendix A Cross-section Oostvaardersdijk

The cross-section measured at the Oostvaardersdijk was showed a confirmation of the lithology provided by the Muskrat Management Zuiderzeeland. From 1 till 17 meter position on the measured radargrams no signal was obtain form the surface as consequent of the clay. The flat and steep bank did show reflections as the soil consisted from sand.

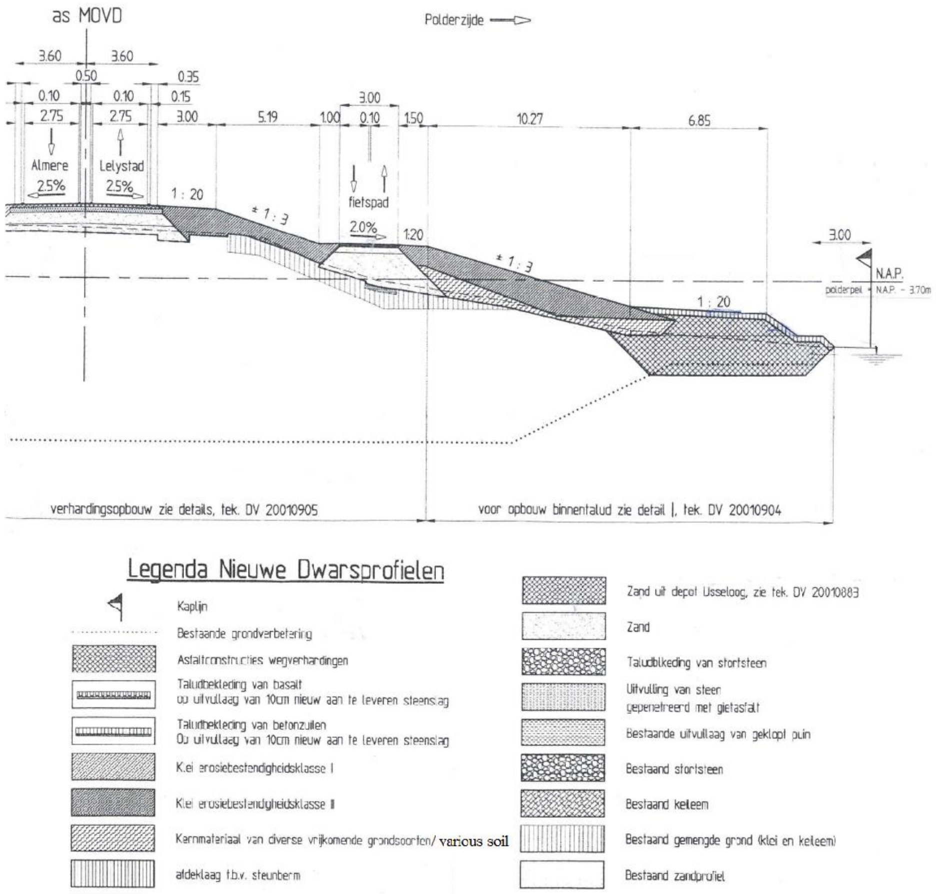

Appendix A.1: Schematic cross-section of the Oostvaardersdijk with legend of the subsurface soil constituents. The survey site differs from the shown cross-section, which has the cycling path (fietspad) at same level as the road in the crest. However it is an indication of the subsurface formations and general layer orientation. (Rijkswaterstaat 2002)

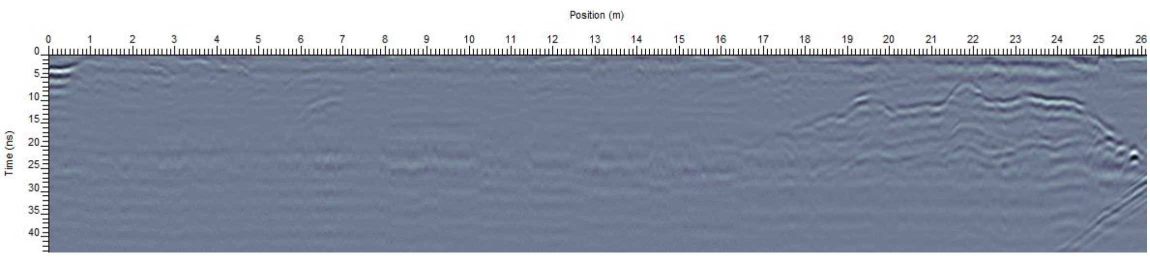

Appendix A.2: 500 MHz antenna radargram of the cross-section of the Oostvaardersdijk, taken from the side of the cycling path on the crest till entrance of a tunnel at the edge of the waterside. See text for detailed interpretation.

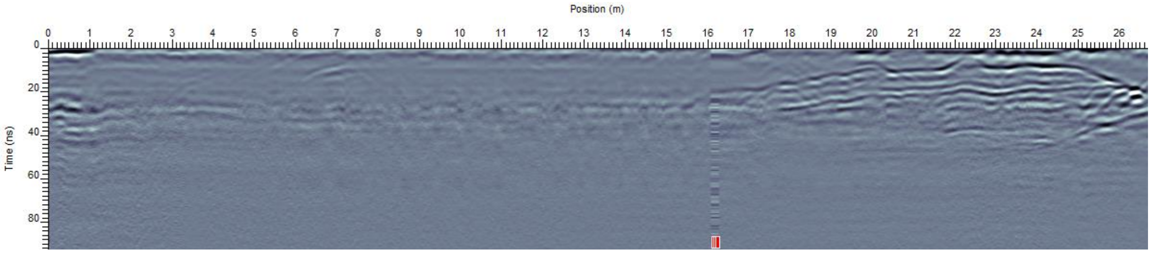

Appendix A.3: 250 MHz antenna radargram showing a similar image as the 500 MHz but a longer time scale and less resolution in the first 30 ns. At 16 m position traces are skipped, indicated on the bottom in red, possible due to loss of contact of the odometer wheel at the transition from steep to flat slope.

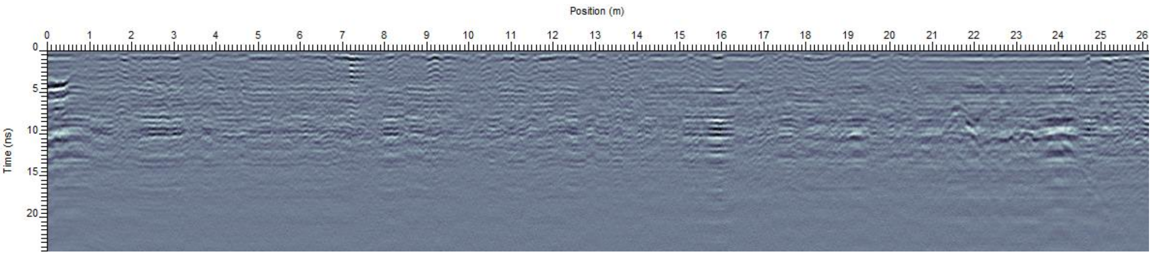

Appendix A.4: Radargram as result of the 1000 MHz is dominated by noise due to ringing and multiples from the ground contact. No clear reflections are visible to be interpreted.

Appendix B Influence of SEG2-gain parameters

The attenuation, start value of the gain, and maximum gain value are parameters that influence the effect of the SEG2-gain applied on the GPR data. The resulting radargrams of the parameters as has been discussed in Chapter 7 are shown below.

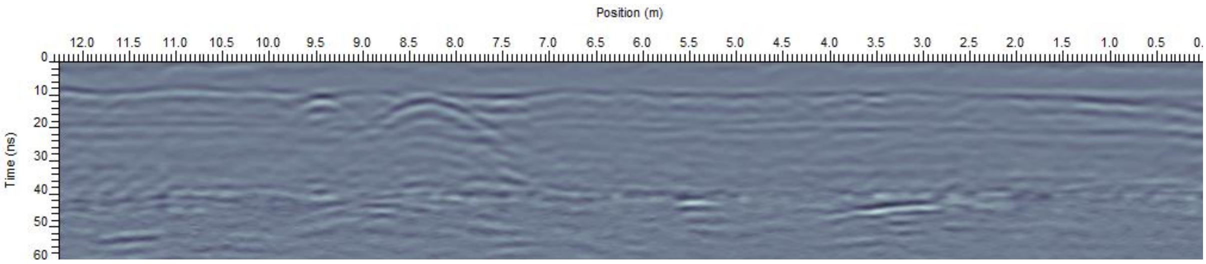

Appendix B.1: Radargram of Figure 19D with applied processing: dewow, background removal and SEG2 gain with attenuation = 11.35, start gain = 1, maximum gain = 477

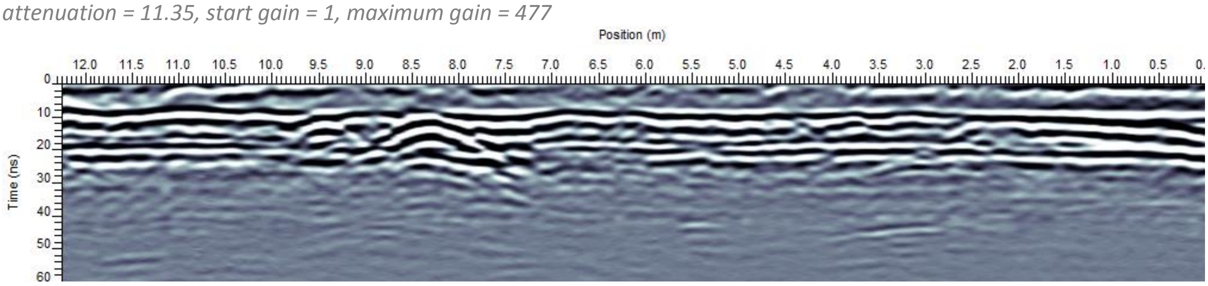

Appendix B.2: Radargram of Figure 19E with applied processing: dewow, background removal and SEG2 gain with attenuation = 11.35, start gain = 15, maximum gain = 477

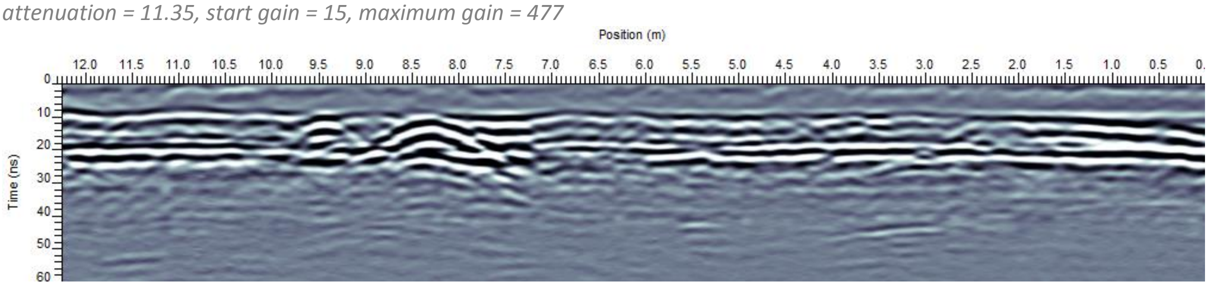

Appendix B.3: Radargram of Figure 19F with applied processing: dewow, background removal and SEG2 gain with attenuation = 20, start gain = 4.49, maximum gain = 477

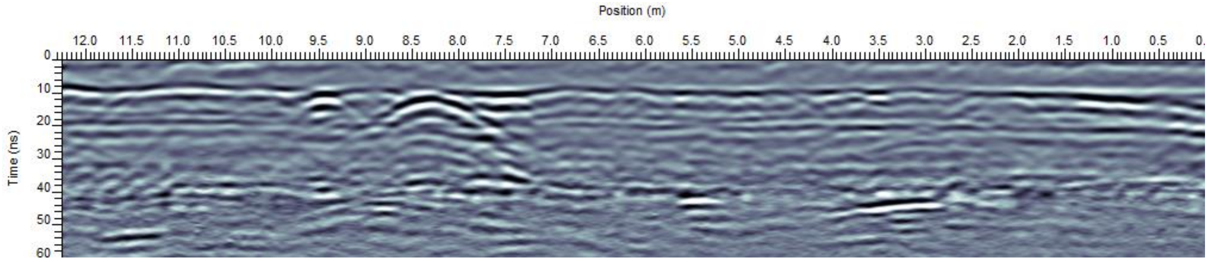

Appendix B.4: Radargram of Figure 19G with applied processing: dewow, background removal and SEG2 gain with attenuation = 11.35, start gain = 4.49, maximum gain = 1500

Appendix C Apparent resistivity section of the Wenner survey

The measured apparent resistivity has been inverted similar to the Dipole-Dipole survey with parameters as has been discussed in Chapter 7.

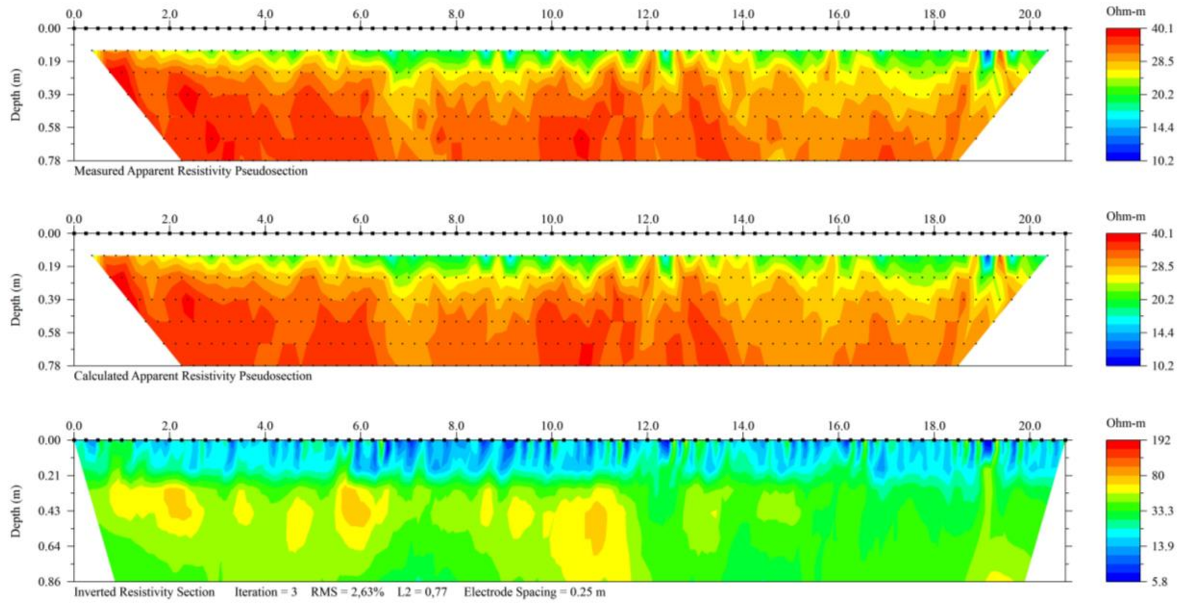

Appendix C.1: Measured, calculated and inverted sections of the Wenner survey. Parameters for inversion were a maximum RMS of 3% and a smoothing and damping factor of 10. Forward modelling was performed with the finite element method, using a Cholesky Decomposition forward solver equation and a mixed boundary condition.

Appendix D Alblasserwaard Location 1 raw data

The original radargram survey with the 500 MHz antenna without interpretation applied.

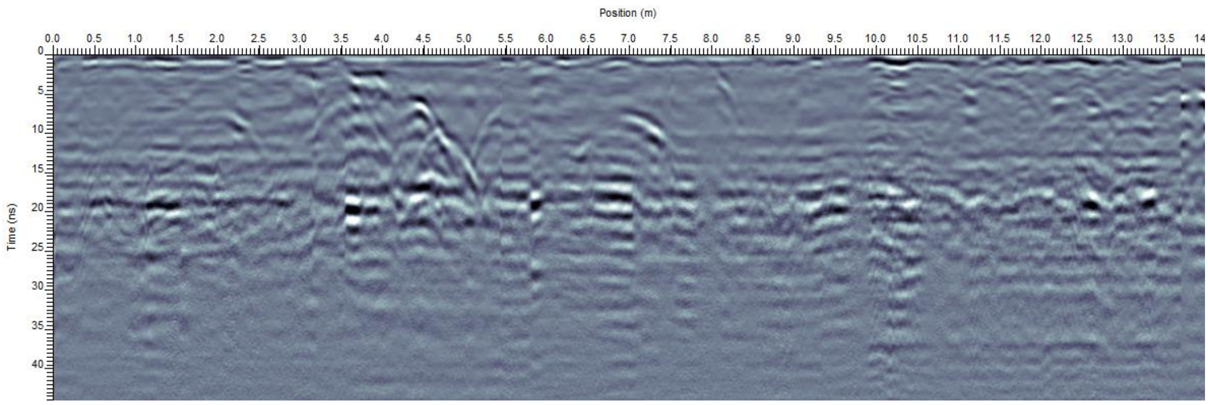

Appendix D.1: Original radargram of Figure 65, survey line at Location 1 measured with the 500 MHz antenna. Red velocity estimation and green highlighted hyperbolic reflections are not shown.